blood

Prepublished online November 19, 2014;
doi:10.1182/blood-2014-06-585299

Cell rigidity and shape override CD47's 'Self' signaling in phagocytosis by hyperactivating Myosin-II

Nisha G. Sosale, Tahereh Rouhiparkouhi, Andrew M. Bradshaw, Rumiana Dimova, Reinhard Lipowsky and Dennis E. Discher

Blood (print ISSN 0006-4971, online ISSN 1528-0020), is published weekly by the American Society of Hematology, 2021 L St, NW, Suite 900, Washington DC 20036.

Blood First Edition Paper, prepublished online November 19, 2014; DOI 10.1182/blood-2014-06-585299

Scientific Section Designation: Red Cells, Iron and Erythropoiesis

Cell Rigidity and Shape override CD47's 'Self' signaling in Phagocytosis by Hyperactivating Myosin-II

Nisha G. Sosale[1], Tahereh Rouhiparkouhi[2], Andrew M. Bradshaw[1], Rumiana Dimova[2], Reinhard Lipowsky[2], and Dennis E. Discher[1*]

1. Molecular & Cell Biophysics Lab, University of Pennsylvania, Philadelphia, PA.
2. Max Planck Institute of Colloids and Interfaces, Potsdam, Germany.
*correspondence: discher@seas.upenn.edu

Total text word count: **3700**
Abstract word count: 200
Figure count: 6 + 5 supplemental
Table count: 2
Reference count: 75

Correspondence: Dennis E. Discher, University of Pennsylvania, 220 S. 33rd Street, 129 Towne Building, Philadelphia, PA 19104, USA; email: discher@seas.upenn.edu.

Submitted [date]; accepted [date]. Republished online as *Blood* First Edition Paper [date]; DOI 10.1182/blood-YYY-MM-NNNNNN.

The online version of the article contains a data supplement.

Key Points

- Rigidity of an opsonized red cell contacting a macrophage hyperactivates myosin-II to overpower CD47's self signaling.

- Red cell shape modulates CD47's signaling of self and highlights biophysical contributions to phagocytosis.

Abstract

A macrophage engulfs another cell or foreign particle in an adhesive process that often activates Myosin-II, unless the macrophage also engages 'Marker of Self' CD47 that inhibits Myosin. For many cell types, adhesion-induced activation of Myosin-II is maximized by adhesion to a rigid rather than a flexible substrate. Here we demonstrate that rigidity of a phagocytosed cell also hyperactivates Myosin-II, which locally overwhelms 'Self' signaling at a phagocytic synapse. Cell stiffness is one among many factors including shape that can change in senescence and in diseases ranging from inherited anemias and malaria to cancer. Controlled stiffening of normal human RBCs in different shapes does not compromise CD47's interaction with the macrophage 'Self'-recognition receptor, SIRPA. Uptake of antibody-opsonized RBCs is always fastest with rigid RBC-Discocytes that also show maximal active Myosin-II at the synapse can dominate 'Self' signaling by CD47. Rigid but rounded RBC-Stomatocytes signal 'Self' better than rigid RBC-Discocytes, highlighting the effects of shape on CD47 inhibition. Physical properties of phagocytic targets thus regulate 'Self' signaling, as is relevant to clearance of rigid RBCs after blood storage, clearance of rigid pathological cells such as thalassemic or sickle cells, and even to interactions of soft/stiff cancer cells with macrophages.

(198 words)

INTRODUCTION

Factors that promote the cytoskeleton-intensive process of phagocytosis (**Fig.1A, left**) are opposed by several inhibitory factors[1] that ultimately dictate whether a macrophage engulfs a target cell or particle. Immunoglobulin-G (IgG) bound to a target engages Fcγ Receptor on a macrophage, for example, and coordinates the assembly of numerous phagocytic synapse proteins[2–4] including nonmuscle myosin-II motors that help drive uptake[5–7]. If CD47 is displayed in parallel on a target, it binds the macrophage's inhibitory receptor SIRPA[8], which activates the immunomodulatory phosphatase SHP-1[9], that regulates multiple proteins[10], including inhibition of nonmuscle myosin-IIA[11]**.** Inhibition of actomyosin contractility at the phagocytic synapse[7,12] could explain various observations that 'Marker of Self' CD47 partially blocks phagocytosis of mouse-RBCs[13] as well as normal white blood cells,[14,15] stem cells,[16] and cancer cells[16,17]. Macrophage uptake of opsonized RBCs is also reported to contribute to clearance of RBCs in senescence[18–23] and in various diseases, including sickle cell anemia and thalassemia[24,25]. Such diseased cells and other conditions, including aging of cells, are the cause of many differences from normal that include increased cell rigidity[26–28], increased IgG opsonization, increased phagocytosis, and *in vivo* processes consistent with increased clearance (**Table S1**). Cell stiffness also changes in cancers and chemotherapy[29–31], which could be important to broad anti-cancer efforts aiming to exploit CD47-SIRPA interactions[12,17]. Particle studies indeed show that stiff gel particles are engulfed in greater numbers than soft particles[32], but relevance to cells with or without 'self' is untested. Normal human RBCs are controllably stiffened here in order to assess phagocytosis of rigid 'self' cells under conditions that aim to preserve the interfacial biochemistry (**Fig.1A, right**).

As RBCs senesce, aldehydes are produced, which greatly accelerates RBC clearance from the circulation, but aldehyde levels are also higher in some diseased cells[33,34]. Aldehydes react primarily with amines in Lys residues, which only occur in CD47 distal to its binding site with SIRPA (PDB: 2JJS). However, aldehydes can sometimes react with Arg,[35] which CD47 has in its binding site (Arg103), so that 'Marker of Self' interactions might be inhibited by reaction with age-generated aldehydes. Aldehyde-mediated crosslinking of various RBC membrane proteins certainly stiffens cells[33]. Rigid RBCs in healthy or disease states become stuck in narrow capillaries throughout the body[36,37], especially splenic slits that impede rigid RBCs[38]; this could facilitate probing and clearance by splenic macrophages[39]. Synthetic polymer 'RBC mimics' that lack any CD47 or other RBC proteins are also removed from circulating blood more rapidly when stiff compared to soft[40].

Rigid cell enlodgement within blood vessels versus rigidity-enhanced phagocytosis have not been distinguished in past studies, and any role for CD47 is also unclear. The hypothesis examined here is that cell rigidity promotes phagocytic uptake by overwhelming CD47's signaling of 'Self'. Mechanistically, in the adhesion of most cell types to a planar substrate, a stiffer substrate generally activates myosin-II moreso than a soft substrate; and such activation drives polarization in hematopoietic stem cells[41], cell spreading of macrophages[42] and neutrophils[43], and actomyosin stress fiber assembly in various fibroblastic cell types[44]. However, whether rigidity driven macrophage activation affects CD47 inhibition of phagocytosis has not been studied. Myosin-II is shown here to be hyperactivated by RBC rigidity and to oppose CD47's 'Self' signaling, thereby increasing phagocytosis. The findings are broadly relevant to accelerated senescence and clearance after blood storage[45], to anemias that affect red cell shape and rigidity, to phagocytosis of cancer cells, and even to synthetic particles used *in vivo*.

Materials and Methods

Reagents, cell lines, and standard methods are described in supplemental Methods. All blood was collected after informed consent with IRB approval at the University of Pennsylvania. This study was conducted in accordance with the Declaration of Helsinki.

Preparation of RBCs. Fresh RBCs were washed with PBS, incubated with 0-50 mM Glutaraldehyde (GA) for 1 min at RT, and extensively washed. GA-stomatocytes were first swollen with 200 mOsm PBS (30 min) then treated with GA (50 mM, 200 mOsm,1 min, RT).

SIRPA Binding Assay. Soluble SIRPA-Glutathione-S-Transferase fusion (SIRPA-GST) was prepared and used as before with fluorescent anti-GST[44] or else fluorescently labeled with AlexaFluor 546 Maleimide (Life Technologies) (SIRPA-GST-Fluor). SIRPA-GST was incubated with RBC for 30 min at RT. Cells were pelleted and re-suspended in 5% FBS/PBS, and intensity measured by flow cytometry (Becton-Dickinson LSRII).

Phagocytosis Assay by Flow Cytometry. For RBC opsonization, 10 μL packed RBC were incubated with 0-10 μL opsonizing antibody (Table S2), and CD47 blocked with 0-3 μL anti-CD47 (B6H12). After shaking (Argos RotoFlex, 45 min, RT), RBCs were pelleted, and labeled with PKH26 dye (RT, 30 min). THP-1 macrophages incubated with opsonized RBCs for standard phagocytosis assay[7], were isolated for flow cytometry analysis by washing cultures

twice in PBS, 0.5 mL H2O for RBC lysis (1 min), followed by Trypsin incubation (5 min, 37ºC) quenched with RPMI. Macrophages were centrifuged (3000g, 5 min), resuspended with DNA labeling (10 min with Hoechst 33342), centrifuged again and resuspended in 5% FBS/PBS for flow cytometry analysis.

RESULTS

Rigid human RBCs bind SIRPA but are rapidly engulfed

Normal human RBCs that are chemically modified with physiological concentrations of malonyldialdehyde[34] (MDA) or else with glutaraldehyde (GA) display functional CD47 as demonstrated by binding soluble SIRPA-GST as well as a function blocking anti-CD47 (**Fig.1B, S1**). GA is just two carbons longer than MDA and is a common but hazardous disinfectant in the clinic[46,47]. Flow cytometry was used to measure binding and to also show that binding of soluble SIRPA-GST to RBCs could be inhibited by pre-treatment of cells with the anti-CD47 (Fig.1B). Fluorescent SIRPA-GST (SIRPA-GST-Fluor) was used to image native and rigid RBCs (**Fig.1C**), and importantly shows that SIRPA can still bind rigid RBCs, indicating that CD47 is likely folded correctly.

For rabbit-RBC suspensions in fluid shear, the bulk deformability of cells decreases exponentially with aldehyde concentration[33] (**Fig.S2A**). To assess cell-to-cell variability after GA treatment and on a scale similar to a phagocytic cup that forms in RBC engulfment, individual human-RBCs were aspirated here into micropipettes of slightly smaller diameter than the cells (**Fig.1D**). All native RBCs were rapidly aspirated and highly distorted, whereas GA-RBC always entered more slowly, deformed less, and with extreme GA treatment became stuck at the micropipette entrance (Fig.1D**, Fig.S2B**). The exponential decrease in single cell deformability index with GA is consistent with past bulk results for aldehyde-treated RBC in shear[33] (Fig.S2A), and the reasonably small cell-to-cell variations indicate uniformity of the reaction. In addition, RBC stored at room temperature for 1.5 days led to cell rigidification similar to a 17 mM GA treatment (Fig 1D, gray triangle). Such storage treatment is not as extreme as time-and-temperature treatments that are already known to drive rapid clearance by the spleen (i.e. refrigerating at 4ºC for >1 mo or heating of RBCs to 50ºC for 20 min[38]).

Fresh RBC-discocytes normally possess a highly flexible membrane that extends easily under forces that even a few myosin motors might apply (~10 pico-Newtons[27,48]). Time-lapse imaging of human-RBCs opsonized with anti-human-RBC antiserum during engulfment by human-

derived THP1 macrophages showed that CD47-blocked RBCs undergo 'classical' phagocytosis, with uptake complete within five minutes after contact (**Fig.2A**). Erythrophagocytosis always begins with a macrophage pinching the RBC membrane into a semi-conical synapse and causing the rest of the discocyte to become more spherical (**Fig.2A,B,S3A**). Such pinching is also evident at the outset of phagocytosis of giant lipid vesicles that are subsequently ruptured (**Fig.S3B**). With RBCs, macrophage pseudopods zipper along the membrane, constricting the erythrocytes in a manner expected to pressurize the hemoglobin-filled cytoplasm. Myosin-IIA contributes to cytoskeletal dynamics beneath the phagocytic cup[6], and confocal imaging confirms that an engulfed RBC is quasi-spherical with a diameter of ~6 μm, consistent with a sphere of conserved volume (Fig.S3A, "engulfed"). When CD47 is not blocked (eg. native RBCs), such engulfment to spherical completion is infrequent (≤25%). More often, as CD47 signals 'Self', macrophage-imposed deformations are larger and more sustained (Fig.2B). GA-discocytes are not deformable and are rapidly engulfed (**Fig.2C**).

Regardless of Self-signaling, extension of native RBCs that are being phagocytosed can provide estimates of forces that macrophages exert in engulfment (**Fig.S3C**). Time-lapse images were quantified most simply in terms of the RBC's projected length (L_p, **Fig.2D**, schematic, top left) along the phagocytosis axis and perpendicular to the synapse. L_p is initially ~8 μm, the diameter of a human-RBC discocyte (Fig.2D). When CD47 is functionally signaling 'Self', L_p increases the most up to ~12 μm, thus stretching the RBC by ~50%. Pseudopods extend from the macrophage but do not surround the RBC at the distal end; the RBC deformation process seems similar to that reported for macrophages pre-treated with a myosin-light chain kinase inhibitor[6] – which will prove to be no coincidence. With GA-rigidified RBC, the RBC is often flipped up and very rapidly engulfed, suggestive of rigidity-enhanced phagocytosis seen previously with polymer beads[32]. The GA-RBCs contact the macrophage *en face* and seem to strongly adhere, but consistent with these GA-discocytes being rigid they do not become fully sphered in the phagosome as occurs with native RBC (Fig.2C, inset fourth panel). GA-discocytes are more often engulfed into spacious phagosomes with ≤3 μm gap between discocyte and phagosome membranes (**Fig.S3D**). The frequency of 'classical' phagocytosis events, in which engulfment vectors inward and the RBC does not greatly stretch, is 100% for GA-discocytes and 75% for CD47-blocked native RBCs *versus* ≤25% for native RBCs signaling 'Self', with such frequency proportional to engulfment time (**Fig.2E**). Importantly, with native RBCs, the process is most often 'non-classical', with large distensions persisting ~2-fold longer than 'classical' uptake and ~5-fold longer than uptake of rigid RBCs.

Myosin-II localization to the Phagocytic Synapse is promoted by RBC Rigidity

Adhesion to a rigid (*not* soft) substrate for many cell types drives cell spreading with assembly of stress fibers and polarization of nonmuscle myosin-II[41,43,49,50]; and Macrophages are certainly mechanosensitive in adhesion[42,51,52] and phagocytosis[32]. Target rigidity can therefore contribute to the generation of contractile forces during the phagocytosis of foreign cells. Accumulation of myosin-IIA at the phagocytic synapse between THP1 macrophages and opsonized human-RBC is largely inhibited by CD47[7], as reproduced in a comparison of CD47-blocked native hRBC and native hRBC (**Fig.3A,B**). Rigid GA-discocytes, in comparison to native RBC, show significantly greater accumulation of myosin-IIA within the macrophage distal to the human-human phagocytic synapse, and this apparent hyperactivation of contractility is completely inhibited by the myosin-II ATPase inhibitor blebbistatin (Fig.3A,B).

Actomyosin stress fibers are common with cells such as fibroblasts when adherent to rigid substrates, but stress fibers are found in only the occasional macrophage[53] as is evident here in the rare THP-1 cell (**Fig.S4A,B**). Surprisingly, addition of opsonized and rigid GA-discocytes caused a larger fraction of cells to assemble stress fibers unlike when native hRBC were added in identical numbers (**Fig.3C,D**). Compared to native hRBCs that were CD47-blocked, rigid GA-discocytes induced the formation of straight and tensed[54] stress fibers in 4-fold more macrophages, while addition of blebbistatin produced 'relaxed' arcs as seen in similarly treated myocytes[55]. Stress fibers were also induced in macrophages when CD47 was blocked (Fig.S4A). Immunoblots against the myosin-IIA heavy chain in whole cell lysates after phagocytosis indeed show a high molecular weight form of myosin-IIA (**Fig.3D, inset**) that suggests a greater assembly of myosin induced by rigid compared to native RBC (**Fig.S4C**). Rigidity of a phagocytic target thus tends to hyperactivate myosin-IIA in macrophages.

Rigid Discocytes are phagocytosed in greater numbers than flexible Discocytes

While studies above (Figs. 1-3) all indicate engulfment processes depend functionally on RBC rigidity and CD47, complete engulfment is the definitive end-stage and must be quantified. In addition, varying the level of opsonization is needed to demonstrate the net balance for and against phagocytic uptake. RBCs in dogs and humans are opsonized by autologous IgG[56] that increases up to 7-fold towards the end of the cell's life span *in vivo*[19, 57], and aged human-RBCs lack other 'eat me' signals such as exposed phosphatidylserine[58]. Engulfment of native human-RBCs by THP1 macrophages is found to increase here with opsonization of the hRBCs by anti-

hRBC antiserum, saturating at >10-fold higher levels than unopsonized hRBC (**Fig.4A**). IgG concentration in serum is 100 μM, and the highest IgG concentration used here has been calculated to be 10 μM with only a minor fraction of this expected to be specific for human RBC (**Table S2**). Direct imaging of engulfed RBCs per macrophage at the end of the 45 min in vitro assay was done by scoring at least 100 randomly chosen macrophages. For higher throughput, a flow cytometry assay was developed (see Methods), and yielded the same relative phagocytic Index as microscopy, with normalization to uptake of native RBCs. Blocking hCD47 nearly doubles the uptake of native cells that are highly opsonized, but blebbistatin inhibition of myosin-II always produces uptake levels statistically similar to native hRBCs (**Fig.4B, left**). Rigidified GA-discocytes are engulfed at similar levels as CD47-blocked native RBCs (**Fig.4B, right**), while decreasing the GA treatment decreases phagocytosis (**Fig.S4D**), similar to previously published results with Malonyldialdehyde (**Fig.S4E**), and follows an exponential trend consistent with the aldehyde-dependence of rigidification (Fig.1D) and *in vivo* clearance (Fig.S2A). Remarkably, blocking CD47 on the rigid GA-discocytes consistently shows no effect on engulfment (Fig.4B-right, **Fig.S4F**). In contrast, blebbistatin always inhibits uptake of GA-Discocytes (Fig.4B, far right), with phagocytosis reduced to levels similar to native RBCs that signal 'Self'. Increased uptake of GA-Discocytes and CD47-Blocked RBCs thus depends largely on active myosin-II.

Varying the level of opsonization by antiserum helps reveal the mechanistic interplay of rigidity sensing and CD47 signaling (**Fig.S4G,H**). At high antiserum opsonization (Table S2, **Fig.4C-i**), increasing amounts of anti-CD47 blocking promotes engulfment of native RBCs, saturating near the invariant level for GA-discocytes. At low antiserum opsonization (**Fig.4C-ii**), engulfment of native RBCs is minimal, with the same increases in anti-CD47 blocking, which indicates that the blocking antibody is not sufficiently abundant to contribute to opsonization. On the other hand, the same low opsonization of GA-discocytes increases engulfment with increasing anti-CD47 (Fig.4C-ii, upper curve). Importantly, because the engulfment curves with anti-CD47 for native hRBCs with high anti-serum (Fig.4C-i) and for rigid RBCs with low anti-serum (Fig.4C-ii) fit to the same saturable uptake curves, hCD47 appears equally functional on GA-treated cells. This conclusion from phagocytosis is consistent with binding to soluble SIRPA-GST (Fig.S1A,C).

For zero anti-serum (**Fig.4C-iii**), engulfment is always much lower, as expected. However, rigid GA-discocytes are again engulfed moreso than native RBC, and blocking with anti-CD47 *decreases* engulfment of rigid GA-discocytes without affecting engulfment of native RBC. The

blocking results for rigid GA-RBC provides additional evidence that CD47 is functional, and since blocking impedes weakly adhesive interactions with macrophage SIRPA[7], the result seems consistent with past reports of CD47 acting as an adhesive ligand for cell tethering and phagocytosis of apoptotic and/or damaged cells[59] – although any cell stiffness in the cited studies were not addressed.

GA-Discocytes with intermediate opsonization (Table S2) were used to clarify the mechanistic balance between pro- and anti-phagocytic signals, starting with pre-incubation of macrophages with an anti-SIRPA antibody that blocks CD47-SIRPA interactions (**Fig.4D**). This leads to engulfment of rigid RBCs that is statistically the same as complete blocking with anti-hCD47. Since CD47 binding to SIRPA activates the phosphatase SHP-1, which we had shown[7] deactivates myosin-IIA at a phagocytic synapse with native RBCs, an inhibitor of SHP-1 (NSC8787712) was added and found to enhance uptake even moreso than the blocking antibodies (Fig.4D). This could reflect a basal level of SIRPA phosphorylation and signaling[7].

We had previously shown NOD/SCID/Il2rg−/− (NSG) mice recognize hCD47 as 'Self', which is evident in slower splenic clearance when hCD47 is displayed[12]. Therefore we injected stiff, highly opsonized hRBC into NSG mice to examine splenic clearance. Blocking or not with anti-hCD47 had no effect on splenic macrophage uptake (**Fig.4E**, **S4I**), which is consistent with our *in vitro* results (Fig.4C).

RBC shape also modulates engulfment

Changes in RBC shape during phagocytosis clearly decrease with RBC stiffness (Fig.2C), but whether the initial shape of the RBC influences engulfment and CD47 signaling is unclear and is certainly relevant to altered RBC shape in hereditary anemias (*e.g.* hereditary spherocytosis and sickle cells[26]); and senescence[22]. Moreover, since rigid polystyrene spheres displaying CD47 can signal 'Self' and inhibit phagocytosis[7,12], we generated and assayed more rounded and rigid RBCs. By treating RBCs with a mild hypotonic buffer prior to GA crosslinking, cells take on a morphology similar to that seen in hereditary stomatocytosis[24, 60] (**Fig.S5A**). In patients, stomatocyte-spleen interactions were abnormally high but also reduced by a drug that decreases production of TNF-a[61], which is often associated with upregulation of adhesion molecules on vascular endothelium[62].

In the absence of opsonization, the hypotonic pre-treatment has no effect on the low basal level of phagocytosis of rigidified cells (**Fig.5A**). However, high antiserum increases phagocytosis in the order Native < GA-Stomatocytes < GA-Discocytes (Fig.5A) even though opsonization is equal across the cells (**Fig.S5B**). The hypotonic treatment is therefore indeed mild rather than damaging. Rigid GA-Stomatocytes bind soluble SIRPA-GST (**Fig.S5C**), and signal 'Self' based on the observation that engulfment numbers increase with anti-CD47 blocking with opsonization by high antiserum (**Fig.5B**) and by purified anti-hRBC IgG (**Fig.S5D**). As with native RBC, immuno-blocking of CD47 on GA-Stomatocytes also increases the rate of engulfment (**Fig.S5E**). Nonetheless, inhibitory signaling with GA-Stomatocytes (Fig.5B) is less effective than that seen with native cells (Fig.4Ci).

With anti-CD47 and high antiserum opsonization, both GA-Discocytes and GA-Stomatocytes are engulfed to a similar extent (Fig.5A). In contrast, GA-Discocytes are engulfed less than GA-Stomatocytes when opsonized with IgG from purified antiserum (Fig.S5D), even though the amount of bound IgG upon Antiserum and Pure IgG opsonization is the same (Fig.S5D, inset). The latter result is consistent with IgG-opsonized "spheres" being phagocytosed more readily than "non-spheres" in studies of particles[63]. The difference may be explained by the fact that antiserum contains additional opsonizing factors, such as C3b[62] that drives complement-receptor mediated phagocytosis characterized by large phagosomes in which the macrophage loosely apposes the target[64-65] and minimizes the dense 'focal' adhesions of IgG-driven phagocytosis[66]. The biconcave contour of a rigid GA-Discocyte, and the resulting non-uniform membrane contact with a macrophage (Fig.S3D) make complement-driven uptake more efficient. The loose contact between macrophage and a GA-Discocyte (Fig.S3D) clearly contrasts with the tightly apposed pseudopods seen during GA-Stomatocyte engulfment (Fig.5B inset).

DISCUSSION

In many disease states and numerous conditions (eg. alcohol consumption), erythrocytes have been amply demonstrated to exhibit increased rigidity, opsonization, and clearance (Table S1), and numerous additional diseases (eg. Fanconi Anemia[67]) have also been speculated to increase RBC rigidity. The quantitative balance between physicochemical changes of RBC that promote phagocytosis *versus* CD47-SIRPA that signals against phagocytosis is summarized in a structure-function heatmap that facilitates objective comparisons of the different phenotypes (columns in **Fig.6A**). The few differences in uptake evident for native RBC *versus* rigid GA-

Discocytes when myosin-II is inhibited most simply reveal uptake of GA-RBC without red cell deformation and also a tendency of GA-Discocytes to stimulate stress fiber assembly even though myosin-IIA's ATPase is inhibited. At the opposite end of the heatmap, blocking of CD47 has little effect on uptake of GA-Discocytes (compare 'CD47-' to 'CD47+'), with a slight attenuation of the uptake phenotype for 'Blocked' cells perhaps reflecting the fact that blocking impedes the weakly adhesive interactions of CD47 with macrophage SIRPA[7]. Native CD47-blocked RBC show an intermediate heatmap profile but group more with the rigid GA-Discocytes, consistent with strong myosin-II activation.

For all of the various RBC targets, IgG on the RBC is likely recognized by the macrophage receptor FcγRIIA, which triggers phagocytic cup formation independent of Myosin-II (**Fig.6B**). The flexible native RBC show that CD47-SIRPA inhibition dominates the opsonization signaling that otherwise activates myosin-II. Blocking CD47 on soft RBCs leads to the characteristic hour-glass deformations seen when native RBC from different species are engulfed[68], consistent with CD47-SIRPA interactions being species specific[7,69,70]. Macrophages cannot deform GA-rigidifed discocytes, which induces Myosin-II activation, assembly, and accumulation at the phagocytic synapse, contributing to rapid rotation of the target in 'en face' ingestion. Loss of RBC deformability contributes to rapid clearance of RBCs from the circulation[33,38], consistent with rapid removal of rigid apoptotic bodies[64,65], but the relative contributions of cell stiffness, opsonin density, and even the roles of macrophages are rarely clear. Rapid uptake can limit signaling from other receptor-ligand interactions as can a rigid discocyte's concave shape, which limits contact between the macrophage's nascent phagosome membrane and a target membrane as shown here (Fig.S3D). A more spherical RBC shape indeed rescues CD47-SIRPA mediated signaling (Fig.5B) consistent with the more tightly apposed projections seen with rounded GA-Stomatocytes (Fig.5B, bottom inset). Rigid polystyrene spheres with CD47 attached likewise signal 'Self', minimizing macrophage uptake *in vitro* and *in vivo* while also suppressing myosin-IIA localization to the phagocytic synapse[7, 12]. FcγR-mediated adhesion seems analogous to the rapid kinase-driven adhesion mediated by integrins that can be amplified into 'focal adhesions' when rigid substrates are engaged by myosin-II contractility [41-44]; however, the slower phosphatase signaling of CD47-SIRPA subsequently benefits from the high contact area and eventually dominates pro-phagocytic processes – unless some threshold for phagocytosis is already crossed in such a kinetic competition mechanism.

The various molecular and cellular processes described here all suggest a myosin-IIA regulatory pathway from unassembled and relaxed states of assembly to contracting fibers that make phagocytosis efficient (**Fig.6C**). Blebbistatin appears to block only the last step (contraction), as imaging after blebbistatin treatment still shows fibers, albeit relaxed fibers (Fig.3C). The CD47 pathway and target rigidity oppositely regulate at least the earlier steps (Fig.6C).

Loss of deformability of aged erythrocytes has long been thought to contribute to their clearance from circulation, with additional determinants possibly including partial 'loss' of CD47 (6-50%[71-73]) and perhaps also oxidation of CD47[74,75]. The results here clarify the complementary role that target deformability plays in clearance by tissue macrophages. The findings are likely relevant to chemotherapy-rigidified leukemias, rigid-walled microbes (yeast and bacteria), various viral and nonviral particles used in gene and drug delivery, and the well-known rigid RBC that result from blood storage and that also occur in common diseases such as sickle cell and thalassemia.

Acknowledgments Support from the NIH (R01-EB007049, R01-HL124106, P01-DK032094, NCATS-8UL1TR000003, P30-DK090969), the NSF (Materials Research Science and Engineering Center, and Nano Science and Engineering Center-Nano Bio Interface Center), and the International Research Training Group (IRTG 1524) is gratefully acknowledged.

Authorship Contributions: NGS, AMB performed experiments; NGS, TR analyzed results. NGS, DED created figures and wrote paper. NGS, RD, RL and DED designed research. Conflict-of-interest disclosure: The authors declare no competing financial interests.

REFERENCES

1 Ravetch JV, Lanier LL. Immune inhibitory receptors. *Science.* 2000;290(5489):84–89.

2 Vincente-Manzanares M, Sanchez-Madrid F. Role of the Cytoskeleton During Leukocyte Responses. *Nat Rev Immunol.* 2004;4(2):110–122.

3 Swanson JA. Shaping cups into phagosomes and macropinosomes. *Nat Rev Mol Cell Biol.* 2008;9(8):639–649.

4 Flannagan RS, Jaumouillé V, Grinstein S. The cell biology of phagocytosis. *Annu. Rev. Pathol.* 2012;7:61–98.

5 Olazabal IM, Caron E, May RC, et al. Rho-Kinase and Myosin-II Control Phagocytic Cup Formation during CR , but Not FcGammaR, Phagocytosis. *Curr Biol.* 2002;12(16):1413–1418.

6 Araki N, Hatae T, Furukawa A, et al. Phosphoinositide-3-kinase-independent contractile activities associated with Fcgamma-receptor-mediated phagocytosis and macropinocytosis in macrophages. *J Cell Sci.* 2002;116:247–257.

7 Tsai RK, Discher DE. Inhibition of "self" engulfment through deactivation of myosin-II at the phagocytic synapse between human cells. *J Cell Biol.* 2008;180(5):989–1003.

8 Jiang P, Lagenaur CF, Narayanan V. Integrin-associated protein is a ligand for the P84 neural adhesion molecule. *J. Biol. Chem.* 1999;274(2):559–562.

9 Veillette A, Thibaudeau E, Latour S. High expression of inhibitory receptor SHPS-1 and its association with protein-tyrosine phosphatase SHP-1 in macrophages. *J Biol Chem.* 1998;273(35):22719–22728.

10 Okazawa H, Motegi S, Ohyama N, et al. Negative regulation of phagocytosis in macrophages by the CD47-SHPS-1 system. *J Immunol.* 2005;174(4):2004–2011.

11 Baba T, Fusaki N, Shinya N, et al. Myosin is an in vivo substrate of the protein tyrosine phosphatase (SHP-1) after mIgM cross-linking. *Biochem Biophys Res Commun.* 2003;304(1):67–72.

12 Rodriguez PL, Harada T, Christian DA, et al. Minimal "Self" peptides that inhibit phagocytic clearance and enhance delivery of nanoparticles. *Science.* 2013;339(6122):971–975.

13 Oldenborg PA, Gresham HD, Lindberg FP. CD47-Signal Regulatory Protein α (SIRPalpha) Regulates Fcgamma and Complement Receptor–Mediated Phagocytosis. *J Exp Med.* 2001;193(7):855–861.

14 Gardai SJ, McPhillips KA, Frasch SC, et al. Cell-surface calreticulin initiates clearance of viable or apoptotic cells through trans-activation of LRP on the Phagocyte. *Cell.* 2005;123(2):321–334.

15 Blazar BR, Lindberg FP, Inguli E, et al. CD47 (integrin-associated protein) engagement of dendritic cell and macrophage counterreceptors is required to prevent the clearance of donor lymphohematopoietic cells. *J Exp Med.* 2001;194(4):541–549.

16 Jaiswal S, Jamieson CH, Pang WW, et al. CD47 Is Upregulated on Circulating Hematopoietic Stem Cells and Leukemia Cells to Avoid Phagocytosis. *Cell.* 2009;138(2):271–285.

17 Weiskopf K, Ring AM, Volkmer JP, et al. Engineered SIRPα variants as immunotherapeutic adjuvants to anticancer antibodies. *Science.* 2013;341(6141):88–91.

18 Kay MM. Mechanism of removal of Senescent cells by human macrophages in situ. *Proc Natl Acad Sci U S A.* 1975;72(9):3521–3525.

19 Turrini F, Arese P, Yuan J, et al. Clustering of integral membrane proteins of the human erythrocyte membrane stimulates autologous IgG binding, complement deposition, and phagocytosis. *J Biol Chem.* 1991;266(35):23611–23617.

20 Oldenborg PA, Zheleznyak A, Fang YF, et al. Role of CD47 as a marker of self on red blood cells. *Science.* 2000;288(5473):2051–2054.

21 Lutz HU. Innate Immune and Non-Immune Mediators of Erythrocyte Clearance. *Cell Mol Biol.* 2004;50(2):107–116.

22 Bosman GJ, Werre JM, Willekens FL, et al. Erythrocyte ageing in vivo and in vitro: structural aspects and implications for transfusion. *Transfus Med.* 2008;18(6):335–347.

23 Hod EA, Zhang N, Sokol SA, et al. Transfusion of red blood cells after prolonged storage produces harmful effects that are mediated by iron and inflammation. *Blood.* 2010;115(21):4284–4292.

24 Mohandas N, Gallagher PG. Red cell membrane: past, present, and future. *Blood.* 2008;112(10):3939–4398.

25 Reliene R, Mariani M, Zanella A, et al. Splenectomy prolongs in vivo survival of erythrocytes differently in spectrin / ankyrin- and band 3 – deficient hereditary spherocytosis. *Blood.* 2002;100(6):2208-2215.

26 Chasis JA, Mohandas N. Erythrocyte Membrane Deformability and Stability: two distinct membrane properties that are independently regulated by skeletal protein associations. *J Cell Biol.* 1986;103(2):343–350.

27 Mohandas N, Evans E. Mechanical Properties of The Red Cell Membrane in Relation to Molecular Structure and Genetic Defects. *Annu Rev Biophys Biomol Struct.* 1994;23:787–818.

28 Raat NJ, Ince C. Oxygenating the microcirculation: the perspective from blood transfusion and blood storage. *Vox Sang.* 2007;93(1):12–8.

29 Bercoff J, Chaffai S, Tanter M, et al. In vivo breast tumor detection using transient elastography. *Ultrasound Med. Biol.* 2014;29(10):1387–1396.

30 Lam WA, Rosenbluth MJ, Fletcher DA. Chemotherapy exposure increases leukemia cell stiffness. *Blood.* 2007;109(8):3505–3508.

31 Cross SE, Jin YS, Rao J, et al. Nanomechanical analysis of cells from cancer patients. *Nat Nanotechnol.* 2007;2(12):780–783.

32 Beningo KA, Wang YL. Fc-receptor-mediated phagocytosis is regulated by Mechanical Properties of the Target. *J. Cell Sci.* 2002;115:849–56.

33 Jain SK, Mohandas N, Clark MR, et al. The effect of malonyldialdehyde, a product of lipid peroxidation, on the deformability, dehydration and 51Cr-survival of erythrocytes. *Br. J. Haematol.* 1983;53(2):247–255.

34 Hebbel RP, Miller WJ. Phagocytosis of sickle cell erythrocytes: immunologic and oxidative determinants of hemolytic anemia. *Blood*. 1984;64(3):733-741.

35 Salem M, Mauguen Y, Prangé T. Revisiting glutaraldehyde cross-linking: the case of the Arg-Lys intermolecular doublet. *Acta Crystallogr Sect F Struct Biol Cryst Commun.* 2010;66:225–228.

36 Ballas SK, Mohandas N. Pathophysiology of Vaso-Occlusion. *Hematol Oncol Clin North Am.* 1996;10(6):1221–1239.

37 Tsai M, Kita A, Leach J, et al. In vitro modeling of the microvascular occlusion and thrombosis that occur in hematologic diseases using microfluidic technology. *J Clin Invest.* 2012;122(1):408–418.

38 Deplaine G, Safeukui I, Jeddi F, et al. The sensing of poorly deformable red blood cells by the human spleen can be mimicked in vitro. *Blood.* 2011;117():88–95.

39 Mebius R E, Kraal G. Structure and function of the Spleen. *Nat Rev Immunol.* 2005;5(8):606–16.

40 Merkel TJ, Jones SW, Herlihy KP, et al. Using mechanobiological mimicry of red blood cells to extend circulation times of hydrogel microparticles. *Proc Natl Acad Sci U S A.* 2011;108(2):586–591.

41 Shin J, Buxboim A, Spinler KR, *et al.* Contractile Forces Sustain and Polarize Hematopoiesis from Stem and Progenitor Cells. *Cell Stem Cell.* 2014;14(1):81–93.

42 Féréol S, Fodil R, Labat B, et al. Sensitivity of alveolar macrophages to substrate mechanical and adhesive properties. *Cell Motil Cytoskeleton.* 2006;63(6):321–40.

43 Oakes PW, Patel DC, Morin NA, et al. Neutrophil morphology and migration are affected by substrate elasticity. *Blood*. 2009; 114(7):1387–95.

44 Engler AJ, Sen S, Sweeney HL, et al. Matrix elasticity directs stem cell lineage specification. *Cell.* 2006; 126(4):677–689.

45 Hod EA, Brittenham GM, Billote GB, et al. Transfusion of human volunteers with older, stored red blood cells produces extravascular hemolysis and circulating non-transferrin-bound iron. *Blood.* 2011;118(25):6675–6682.

46 Centers for Disease Control and Prevention. 2008; Retrived from http://www.cdc.gov/hicpac/pdf/guidelines/disinfection_nov_2008.pdf

47 Di Stefano F, Siriruttanapruk S, McCoach J, et al. Glutaraldehyde: an occupational hazard in the hospital setting. *Allergy*. 1999;54(10):1105-1109.

48 Li J, Dao M, Lim CT, et al. Spectrin-level modeling of the cytoskeleton and optical tweezers stretching of the erythrocyte. *Biophys J.* 2005;88(5):3707–3719.

49 Lo CM, Buxton DB, Chua GC, et al. Nonmuscle Myosin IIB Is Involved in the Guidance of Fibroblast Migration. *Mol Biol Cell.* 2004;15(3):982–989.

50 Raab M, Swift J, Dingal PC, et al. Crawling from soft to stiff matrix polarizes the cytoskeleton and phosphoregulates myosin-II heavy chain. *J Cell Biol.* 2012;199(4):669–683.

51 Patel NR, Bole M, Chen C, et al. Cell elasticity determines macrophage function. *PLoS One.* 2012;7(9):e41024.

52 Blakney AK, Swartzlander MD, Bryant SJ. The effects of substrate stiffness on the in vitro activation of macrophages and in vivo host response to poly(ethylene glycol)-based hydrogels. *J Biomed Mater Res A.* 2012;100(6):1375–86.

53 Lammel U, Bechtold M, Risse B, et al. The Drosophila FHOD1-like formin Knittrig acts through Rok to promote stress fiber formation and directed macrophage migration during the cellular immune response. *Development*. 2014;141(6):1366-1380.

54 Tanner K, Boudreau A, Bissell MJ, et al. Dissecting regional variations in stress fiber mechanics in living cells with laser nanosurgery. *Biophys J.* 2010;99(9):2775–83.

55 Sen S, Tewari M, Zajac A, et al. Upregulation of paxillin and focal adhesion signaling follows Dystroglycan Complex deletions and promotes a hypertensive state of differentiation. *Eur. J. Cell Biol.* 2011;90(2-3):249–260.

56 Christian JA, Rebar AH, Boon GD, et al. Senescence of canine biotinylated erythrocytes: increased autologous immunoglobulin binding occurs on erythrocytes aged in vivo for 104 to 110 days. *Blood.* 1993;82(11):3469–3473.

57 Rettig MP, Low PS, Gimm JA, et al. Evaluation of Biochemical Changes During in Vivo Erythrocyte Senescence in the Dog. *Blood.* 1999;93(1):376–384.

58 Franco RS, Puchulu-Campanella ME, Barber LA, et al. Changes in the properties of normal human red blood cells during in vivo aging. Am J. Hematol. 2012;88(1):44-51.

59 Tada K, Tanaka M, Hanayama R, et al. Tethering of apoptotic cells to phagocytes through binding of CD47 to Src Homology 2 Domain-Bearing Protein Tyrosine Phosphatase Substrate 1. *J. Immunology.* 2003;171(11):5718-5726.

60 Da Costa L, Galimand J, Fenneteau O, et al. Hereditary spherocytosis, elliptocytosis, and other red cell membrane disorders. *Blood Rev.* 2013; 27(4):167-178.

61 Smith BD, Segel GB. Abnormal Erythrocyte Endothelial Adherence in Hereditary Stomatocytosis. *Blood.* 1997;89(9):3451-3456.

62 Janeway, CA Jr; Travers P, Walport M, et al (2001). *Immunobiology: The Immune System in Health and Disease*. New York: Garland Science.

63 Champion JA, Mitragotri S. Role of target geometry in phagocytosis. *Proc Natl Acad Sci U S A.* 2006;103(13):4930–4934.

64 DeCathelineau AM, Henson PM. The final step in programmed cell death: phagocytes carry apoptotic cells to the grave. *Essays Biochem* 2003;39:105-117.

65 Erwig LP, Henson PM. Clearance of apoptotic cells by phagocytes. *Cell Death Differ*. 2008; 15(2):243-250.

66 Allen L, Aderem A. Molecular Definition of Distinct Cytoskeletal Structures Involved in Complement- and Fc Receptor-mediated Phagocytosis in Macrophages. *J Exp Med.* 1996;184(2):627-637.

67 Malorni W, Straface E, Pagano G, et al. Cytoskeleton alterations of erythrocytes from patients with Fanconi's anemia. *FEBS Lett*. 2000; 468(2-3):125-128.

68 Swanson JA, Johnson MT, Beningo K, et al. A contractile activity that closes phagosomes in macrophages. *J Cell Sci.* 1999;112(3):307-316.

69 Subramanian S, Parthasarathy R, Sen S, et al. Species- and cell type-specific interactions between CD47 and human SIRPA. *Blood.* 2006;107(6):2548–2556.

70 Takenaka K, Prasolava TK, Wang JCY, et al. Polymorphism in SIRPA modulates engraftment of human hematopoietic stem cells. *Nature Immunology* 2007;8(12):1313-1323.

71 Annis AM, Sparrow RL. Expression of CD47 (integrin-associated protein) decreases on red blood cells during storage. *Transfusion and Apheresis Science* 2002;27(3):233-238.

72 Kamel N, Goubran F, Ramsis N, et al. Effects of storage time and leucocyte burden of packed and buffy-coat depleted red blood cell units on red cell storage lesion. *Blood Transfus.* 2010;8(4):260-266.

73 Stewart A, Urbaniak S, Turner M, et al. The application of a new quantitative assay for the monitoring of integrin-associated protein CD47 on red blood cells during storage and comparison with the expression of CD47 and phosphatidylserine with flow cytometry. *Transfusion.* 2005;45(9):1496-1503.

74 Olsson M, Oldenborg PA. CD47 on experimentally senescent murine RBCs inhbits phagocytosis following Fcgamma receptor-mediated but not scavenger receptor-mediated recognition by macrophages. *Blood.* 2008;112(10):4259-4267.

75 Burger P, Hilarius-Stokman P, de Jorte D, et al. CD47 functions as a molecular switch for erythrocyte phagocytosis. *Blood.* 2012;119(23):5512-5521.

Figure Legends

Figure 1. **SIRPA binds CD47 on both rigid and native RBC.** (**A**). Downstream of FcγR binding of IgG, kinases phosphorylate multiple cytoskeletal proteins, including myosin-II, which drive assembly of the phagocytic cup and promote uptake. CD47-SIRPA signaling leads to activation of SHP-1 phosphatase that can deactivate Myosin-II. Since, substrate rigidity initiates assembly and polarization of Myosin-II in many cell types, phagocytic target rigidity is expected to counterbalance CD47-mediated inhibition of the motor. Our working hypothesis is that with flexible self cells (left), CD47 initiated inhibition can overcome myosin-II activation, whereas with rigid self cells (right), the myosin-II driven cytoskeleton is not diminished by CD47-SIRPA 'self' signals. (**B**) Flow cytometry histograms show SIRPA-GST binds to GA- and MDA- rigidified RBCs unless partially blocked by pre-treating RBCs with anti-CD47. Cell aggregation by this antibody prevents a demonstration of complete inhibition. (**C**) SIRPA-GST-Fluor is covalently labeled with fluorophore and binds both native and aldehyde treated RBCs (Scalebar: 5 μm). SIRPA-GST-Fluor was used to bind the MDA-RBCs in panel-B, whereas anti-GST was used to detect binding on native and GA-RBCs. Fig.S1 further illustrates the saturable and specific binding as well as CD47 blocking. (**D**) Aspiration of RBCs into micropipettes with diameters similar to phagocytic cups and *in vivo* capillaries shows GA-treatment rigidifies cells and so does storage at ambient conditions. The maximal RBC length and width under aspiration were quantified by image analysis and normalized by pressure and pipette cross-section (Native: n = 9, 17 mM-GA-Discocyte: n = 23, 50 mM GA-Discocyte: n = 2, error bar = SD). (* $p \leq 0.05$ compare to Native, trendline $R^2 = 0.99$).

Figure 2. **Phagocytic uptake of opsonized RBC is faster with CD47 inhibition but fastest for rigid RBC.** Human-derived THP-1 macrophages were incubated with human-RBCs that were opsonized with anti-hRBC antiserum and also either: (**A**) blocked with anti-CD47, (**B**) Native RBC with active CD47+, or else (**C**) rigidified as GA-Discocytes. Time-lapse imaging in DIC and phase contrast begins with initial adhesion between macrophage and RBC targets, and ends upon complete engulfment. The RBC of interest in each frame is pseudocolored blue, green, or pink (Scale bar: 8 μm). At the right of each of the time-lapse series, silhouettes of the target RBC clarify the changes in RBC morphology over the course of engulfment and RBC position relative to the initial macrophage boundaries, as indicated by the colored lines. (**C, 4th panel, inset**) GA-discocytes are often enclosed in a spacious phagosome that shows gaps between the discocyte and phagosome membranes. (**D**) The projected length (L_p) of the engulfed RBC was quantified along the phagocytosis axis (schematic, top left) and shows that

phagocytic deformation is fast and 'classically' vectored inward for rigid RBCs and for CD47-blocked RBCs compared to native RBCs ($n \geq 3 \pm SD$). When CD47 can signal 'Self', phagocytosis is much slower and L_p often increases (up to 1.5-fold L_{p0}). (**E**) The percentage of classical uptake events for each RBC treatment is plotted versus the time required to complete engulfment, with the frequency of classical uptake showing a negative linear correlation with engulfment time (Line fit: $R^2 = 1.0$). Non-classical uptake is most frequently observed with Native RBCs that signal 'Self' and deviates from the classical trend by ≥2-fold.

Figure 3**. Myosin II Accumulation at the Phagocytic Synapse is strongly promoted by target rigidity and more weakly inhibited by CD47.** (**A**) The phagocytic synapse schematic (left) illustrates the intensity analysis of immunofluorescence images. White arrow indicates alignment. THP-1 macrophages were either pre-treated or not with myosin-II inhibitor Blebbistatin (20 μM), followed by incubation with the various anti-serum opsonized RBCs for 45 min at 37ºC, then fixed and immunostained for Myosin-IIA (green), F-actin (red), and DNA (blue) (Scale bar 10 μm). (**B**) Accumulation of Myosin II at the phagocytic synapse was quantified ($n \geq 3 \pm SD$), proving highest for rigid GA-Discocytes and, secondarily, for CD47-blocked RBC (*$p < 0.05$). Blebbistatin suppresses Myosin-IIA accumulation to levels similar to Native RBC, denoted CD47+ (** $p<0.05$). (**C**) Fluorescence images of Myosin-IIA localization in macrophage fed either GA-Discs with or without pre-treatment with Blebbistatin (20 μM), or CD47-blocked RBC (Scale bar: 30 μm). (**D**) Actomyosin fiber formation was quantified in macrophages, showing that addition of GA-Discocytes resulted in the highest frequency of macrophages with stress fibers. Blebbistatin pre-treated macrophages showed curved and relaxed fibers, whereas macrophages cultured with native RBCs do not show fibers. (**inset**) Immunoblot for nonmuscle myosin IIA heavy chain, of macrophage lysates following phagocytosis, shows the presence of 230 kDa and 520 kDa bands, with the high molecular weight band suggesting stable myosin assembly.

Figure 4. **Rigid RBCs and CD47-Blocked RBCs both promote Opsonization-Driven Phagocytosis unless Myosin II is directly inhibited.** (**A**) Phagocytic uptake shows an increasing and saturating response to anti-serum concentration. “High antiserum” is defined as treatment with antiserum concentration greater than that required to result in half of saturating levels of engulfment, as highlighted by the arrows and red box. (**B**) High antiserum opsonized RBCs were incubated with THP1s for 45 min at 37ºC. A microscopy based phagocytosis assay indicated that native RBC were engulfed moreso when they were CD47-blocked, unless THP1 were pre-treated with blebbistatin (20 μM). Rigidifed GA-Discocyte engulfment proved independent of CD47 blocking (*$p < 0.05$). However, engulfment of GA-Discs, like native RBCs, was inhibited by pre-treating THP1s with blebbistatin. The gray bar thus highlights a baseline level of myosin-II-independent phagocytosis. Phagocytosis is significantly higher than the baseline when RBC targets are either CD47-blocked or GA-rigidified. Blebbistatin pre-treatment of both native-blocked and rigid cells keep uptake at the baseline. (**C**) High-throughput flow cytometry assay for phagocytic uptake with opsonization per Table S2 shows that for *high antiserum opsonization*, phagocytosis of GA-Discocytes is unaffected by blocking of CD47 (**i**, ns), while at *low antiserum opsonization* blocking of CD47 on GA-Discocytes does increase phagocytosis (**ii**). For *high antiserum opsonized* deformable ‘Native RBCs’, phagocytosis increases with blocking of CD47 (i), whereas, at *low antiserum* opsonization, phagocytosis of native cells is insignificant regardless of blocking CD47 (ii, ns). Hyperbolic fits for i and ii give K = 90 nM and ~2.5-fold increase from baseline to saturation. Clearly, the anti-CD47 blocking treatment alone is not sufficient to drive engulfment of Native RBC. In the absence of antiserum, or with *zero antiserum* treatment, blocking CD47 on GA-discocytes reduces phagocytosis (**iii**). This suggests functional CD47-SIRPA interaction on rigidified cells indicated by the SIRPA binding studies here (Fig.1B) (For all experiments, *$p < 0.05$; $n \geq 3 \pm$ SEM). (**D**) At intermediate antiserum opsonization (Table S2), CD47 signaling can be blocked. Phagocytosis of native RBC and rigid GA-discocytes significantly increases upon blocking with anti-CD47 (90 nM). An anti-SIRPA antibody (90 nM) and an SHP-1 inhibitor (NSC87877, 60 nM) enhance uptake of GA-discocytes. (**E**) NSG Splenic Macrophages take up stiff, highly opsonized hRBC *in vivo,* independent of CD47. High antiserum opsonzed GA rigidified (17 mM) RBC were Anti-CD47 (CD47-Block) treated or not (CD47+), mixed 1:1, and injected into NSG mice via the tail vein (n=4). Rigid discs were pre-labeled with two lipophilic dyes, either DiR or PKH26, in order to be distinguished after mixing. Spleens were isolated 15 min post-injection, dissociated and analyzed by flow cytometry. Splenic macrophages were distinguished from splenocytes by Cd11b expression and quantified for the percentage positive for RBC uptake. While 1% of

splenic macrophage were positive for CD47-Blocked and CD47+ hRBCs, doubly positive macrophages were rare as were positive non-macrophage cells (CD11b-).

Figure 5. **Shape of Rigid RBC Modulates CD47's "Don't Eat Me" Signal.** (**A)** A flow cytometry based phagocytosis assay shows that macrophage phagocytosis of high antiserum opsonized native RBC, GA-stomatocytes, and GA-Discs is significantly higher than unopsonized cells (*p < 0.05, compares indicated conditions; ** p<0.05 compares high antiserum to zero antiserum for each RBC condition: Native RBC, GA-Stomatocytes, and GA-Discs). (**B**) RBCs treated with a mild hypotonic buffer followed by GA reaction generated rigid, more rounded, GA-Stomatocytes (B, upper inset image). A flow cytometry based phagocytosis assay of *high antiserum opsonized* GA-Stomatocytes shows less engulfment than GA-Discocytes in the absence of anti-CD47 blocking antibody, while blocking CD47 equalized uptake. (*p < 0.05; n ≥ 5000 macrophage in duplicate, ± SD). Time-lapse imaging of the macrophage phagocytic synapse with the stomatocyte shows pseudopods closely apposed to the rounded cell (B, lower inset image).

Figure 6. **Myosin II Activity at the Phagocytic Synapse with Opsonized RBC Targets is Inhibited by CD47, while Enhanced by Target Rigidity. (A)** Heatmap summary and hierarchical clustering of normalized results for the various experiments. The dendrogram indicates that macrophage response to rigid GA-discocytes is distinct from that of native RBC targets, and that blocking CD47 on deformable RBCs (but not on GA-Discocytes) reduces the difference as does blebbistatin pre-treatment of macrophages encountering GA-Discocytes (CD47+ GA-Disc +Blebb). CD47 inhibition is partially rescued with rigid but rounded GA-stomatocytes (CD47+ GA-Stom), unless CD47-Blocked (CD47- GA-Stom). (**B**) Macrophage recognition of IgG opsonin on the surface of RBC by FcγR phagocytic receptors activates cytoskeletal proteins including Myosin-II. Effective signaling via SIRPA to phosphatases does occur with CD47 on either flexible 'Self' cells or sufficiently rounded but rigid 'Self' cells. RBC rigidity has the effect of rapidly and strongly activating adhesion and myosin-II contractions. Macrophages pinch deformable CD47-blocked native RBCs at their midpoint, and then fully engulf these RBCs in a manner analogous to a deflated balloon pulled through a napkin ring (inset schematic). Rigid discocytes maintain their shape throughout engulfment, which limits contact between macrophage receptors and ligands, particularly SIRPA and CD47 on the RBC, and thus the spacious phagosome may act as a signaling barrier. Rounded GA-stomatocyte show tightly apposed macrophage pseudopods, and rescued CD47-signaling. (**C**) Schematic

of Myosin-II assembly in phagocytosis in which Myosin-II dimers assemble and contract actin filaments in response to rigidity of human RBCs, while becoming more disorganized in response to CD47-SIRPA mediated activation of immunoinhibitory phosphatase, SHP-1. We had shown previously[7] that phosphorylation of tyrosines in myosin-IIA's head and tail activate the motor, increasing its accumulation at the phagocytic synapse and increasing the efficiency of phagocytic uptake, while CD47-SIRPA's activation of the tyrosine phosphatase SHP-1 *de*-activates myosin-IIA. Blebbistatin blocks the activity of myosin II ATPase, and thus the ability of the head to generate contractile forces, relaxing the assembled actomyosin fibers. The SHP-1 inhibitor NSC87877 reduces inhibition by CD47 and thus increases RBC uptake.

Figure 1 SIRPA binds CD47 on both rigid and deformable RBC

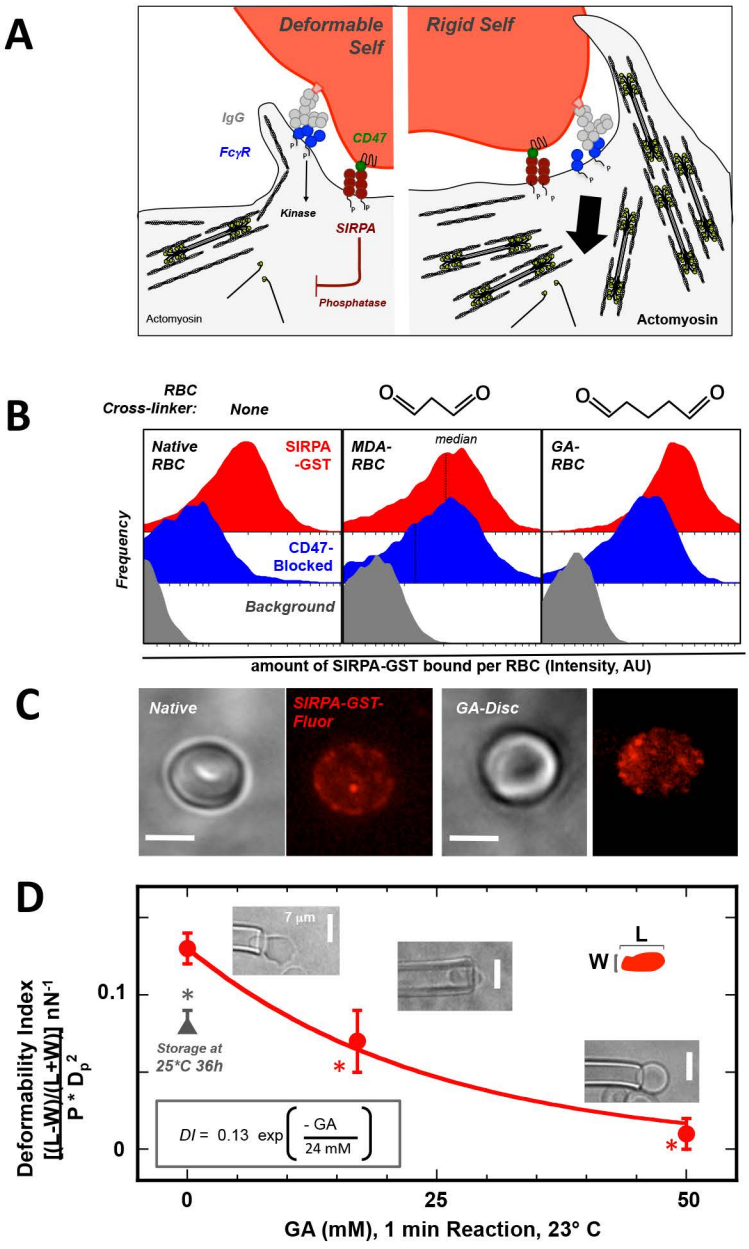

Figure 2 Phagocytic uptake of opsonized RBC is faster with CD47 inhibition but fastest for rigid RBC

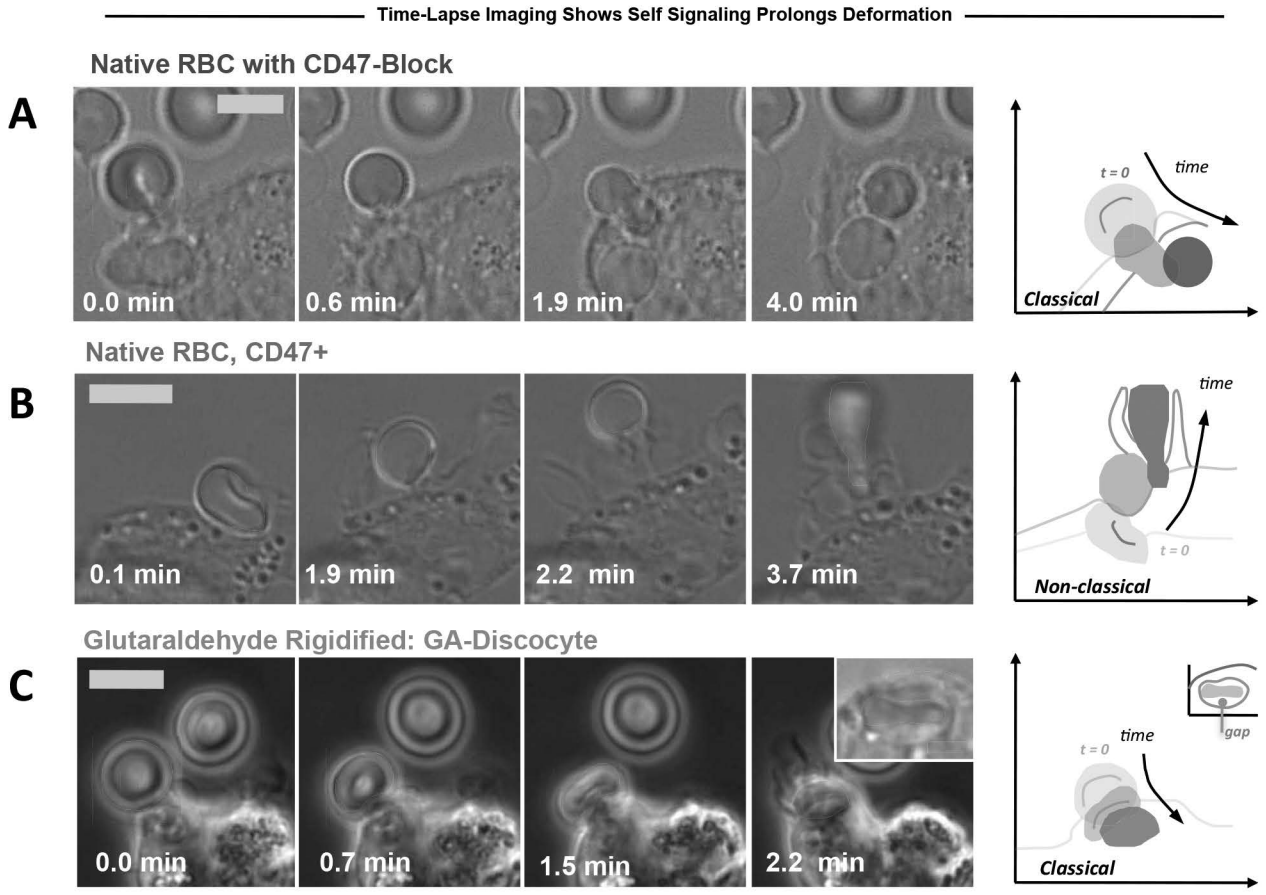

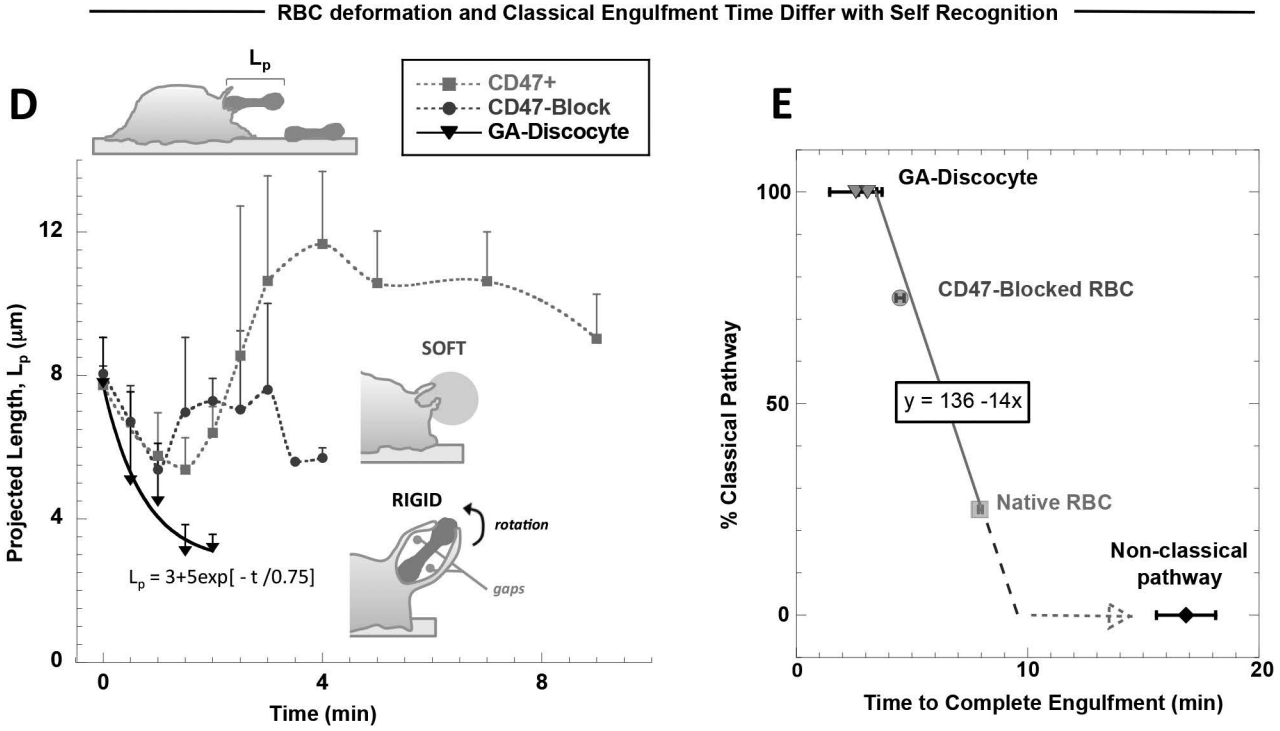

Figure 3 Myosin II Accumulation at Phagocytic Synapse is strongly promoted by target rigidity and more weakly inhibited by CD47

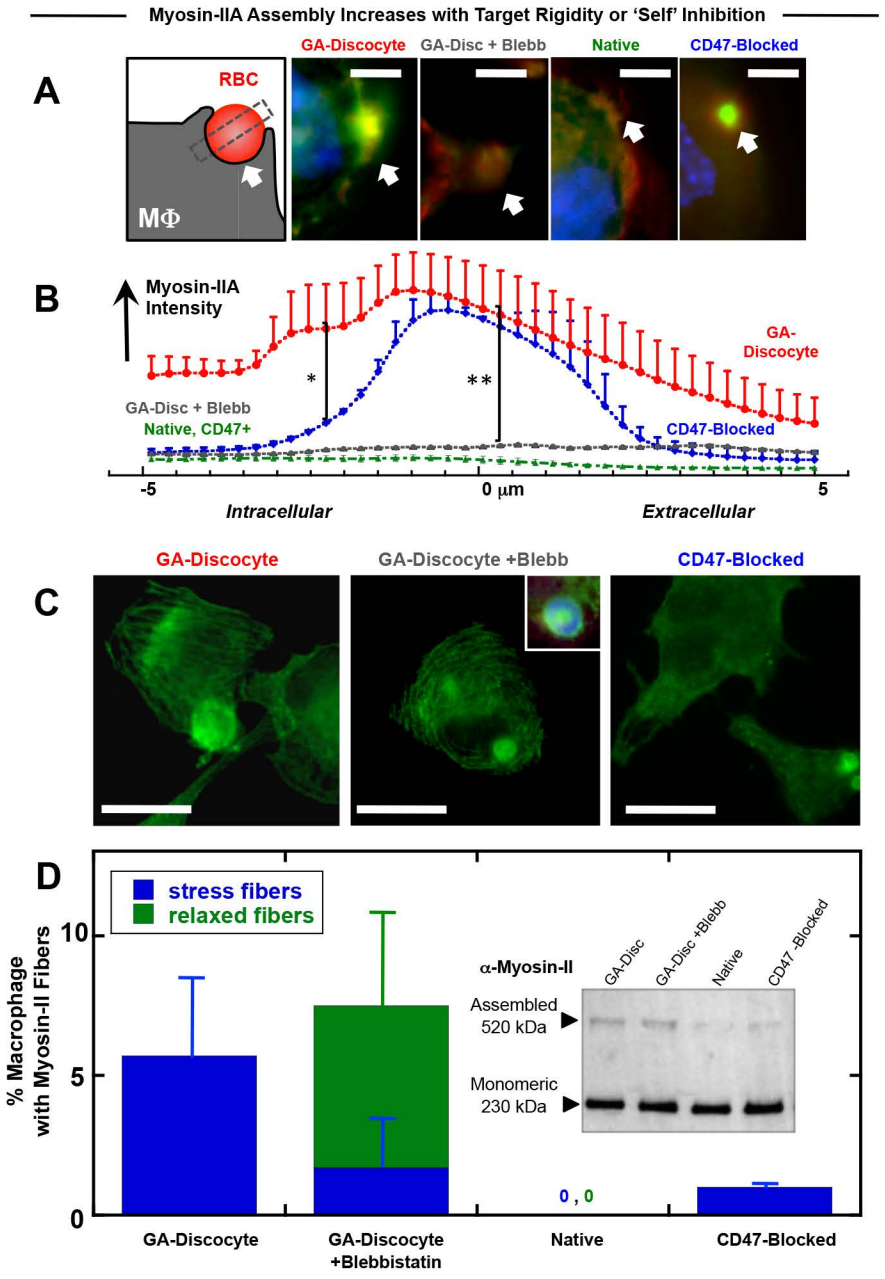

Figure 4 Rigid RBCs & CD47-Blocked RBCs both promote Opsonization-Driven Phagocytosis unless Myosin-II is directly inhibited

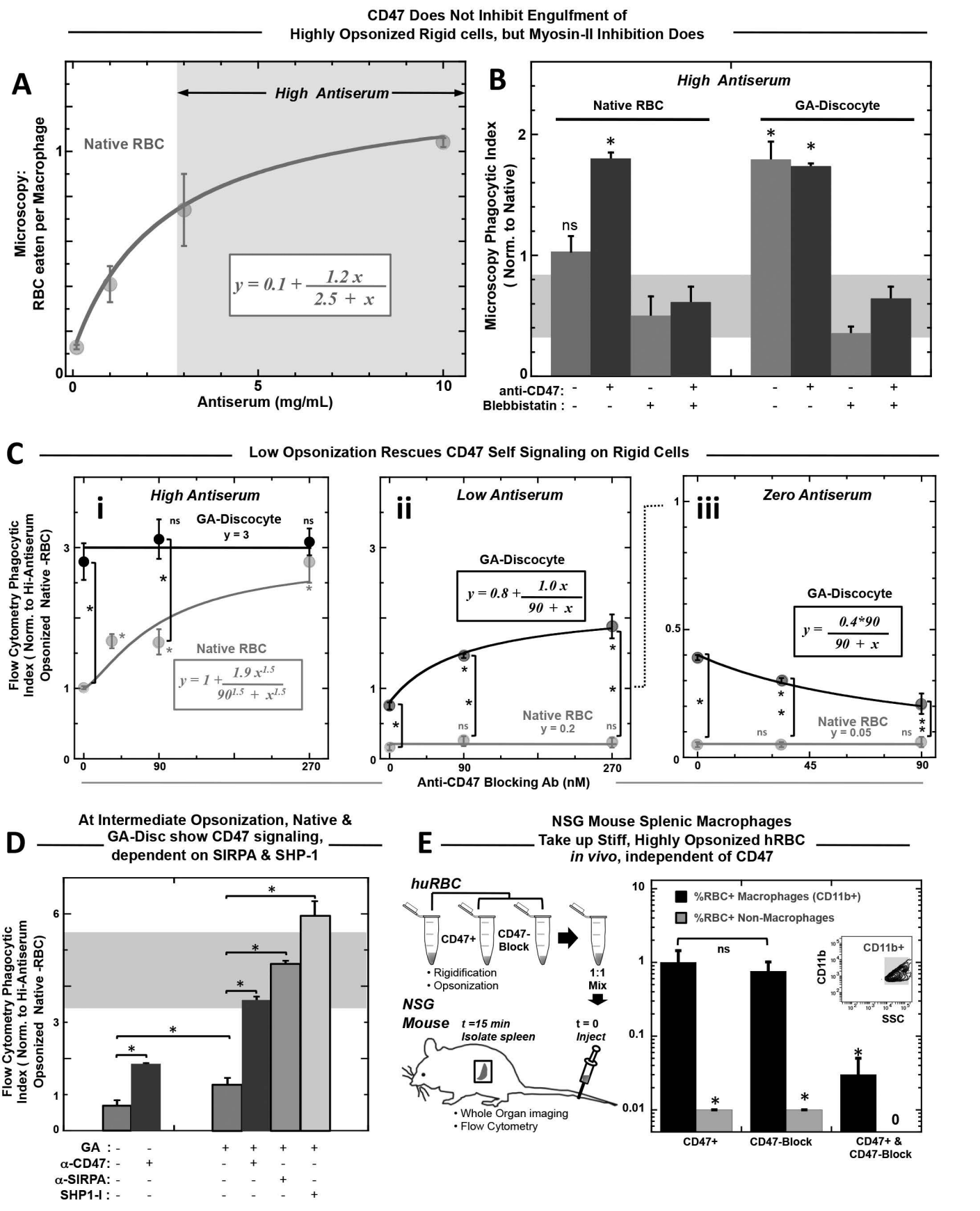

Figure 5 Shape of Rigid RBC Modulates CD47 Signaling

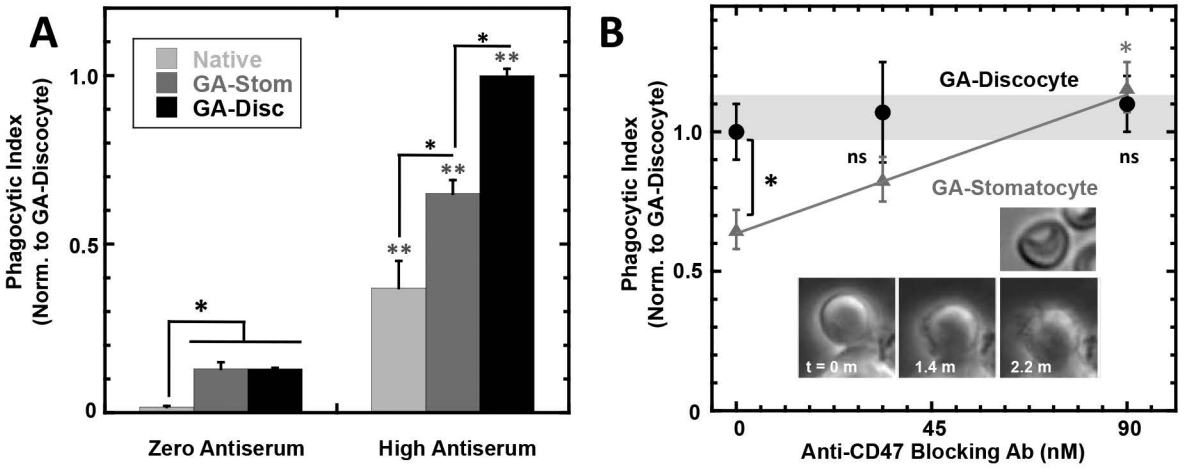

Figure 6 Myosin II Activity at the Phagocytic Synapse with Opsonized RBC Targets is Inhibited by CD47, while Enhanced by Target Rigidity

A

Heatmap Summary of Phagocytic Function and Cytoskeletal Structure :
Rigid, Round Shape Signals 'Self' Better than Rigid Discocyte

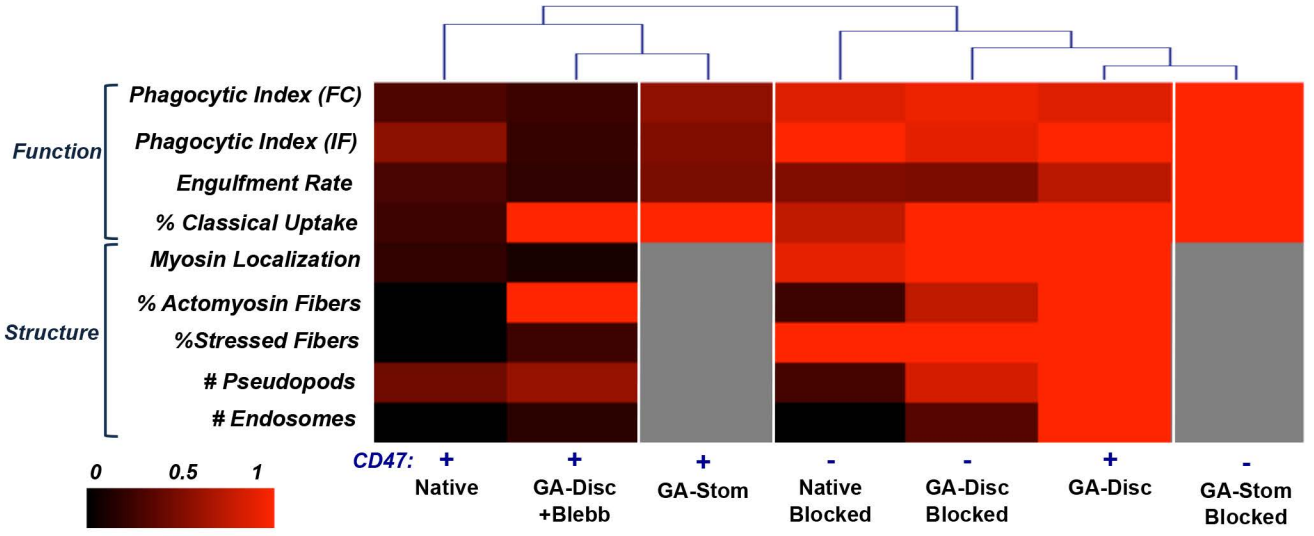

B

Myosin Activation and Engulfment Depend on RBC Rigidity and Shape

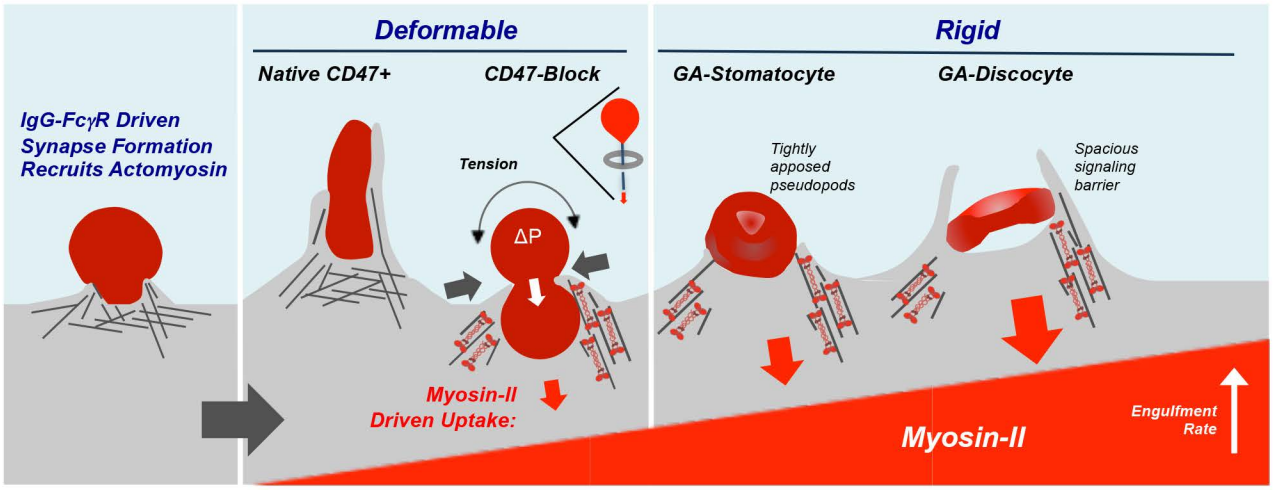

C

Myosin-II Activation: Assembly and Contractility, is Regulated By RBC Rigidity and CD47-SIRPA Signaling

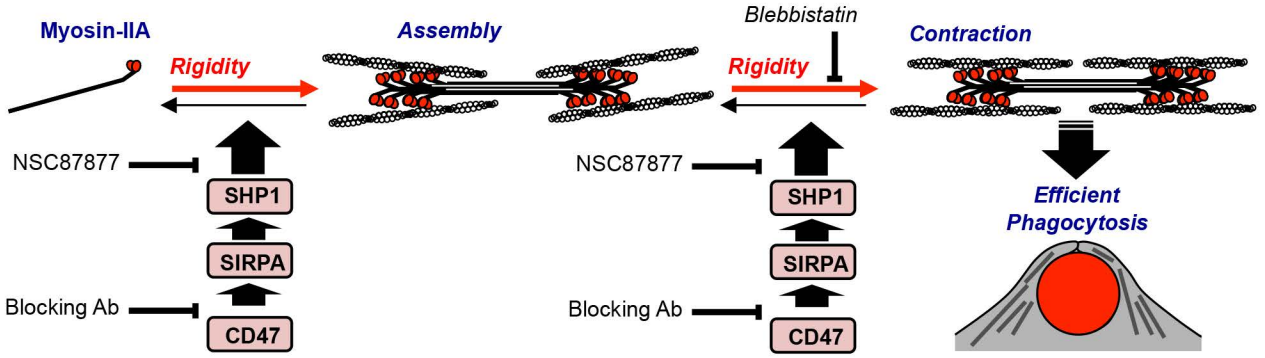

Supplementary Materials and Methods

Cells, Reagents, and Antibodies. THP-1 macrophage (American Type Culture Collection and European Collection of Cell Cultures) were cultured in RPMI (Invitrogen) supplemented with 10% FBS (Sigma). Differentiation of THP-1 cells was achieved in 100 ng/ml phorbol myristate acetate (PMA) (Sigma-Aldrich) for 2 d and confirmed by attachment of cells to culture vessel. For microscopy based phagocytosis assays macrophage were cultured in 4-cm2 Lab-Tek chambered coverglass (Nalge Nunc International), and for flow based phagocytosis assays macrophage were cultured in 6-well plastic dishes (Corning). Dulbecco's phosphate-buffered saline (DPBS) without Ca2+ or Mg2+ (Invitrogen) was supplemented or not with BSA (Sigma-Aldrich). PKH26 (Sigma-Aldrich) was used for RBC labeling. RBC opsonins included Anti-human RBC antibody (rabbit, Rockland Pharmaceuticals) and Anti-human RBC IgG (rabbit, Rockland Pharmaceuticals) (Table S2). Anti-CD47 mAb clone B6H12 (BD Biosciences) was used to block CD47. Secondary antibodies used to detect bound opsonins included Donkey Anti-rabbit IgG conjugated with AlexaFluor 488 or AlexaFluor647. Anti-Myosin IIa was used in IF of the Phagocytic synapse (mouse, Abcam). Anti-Myosin IIa (rabbit, Sigma) was used in actomyosin fiber analyses and western blotting. Hoechst 33342 (Invitrogen) was used to identify the macrophage nucleus. Reagents used to detect F-actin included Phalloidin conjugated with AlexaFluor 488 (Invitrogen) or TRITC (Sigma). Racemic Blebbistatin was used in phagocytosis assays (EMD Biosciences).

Micropipette Aspiration. Capillary tubes were pulled into micropipettes and trimmed by microforge (Vibratome) to mean diameter ~6 mm. Micropipettes were attached to a dual-stage water manometer with adjustable height reservoirs. Suction was applied by syringe, and pressure measured by transducer (Validyne). Pipettes pre-rinsed with 3% BSA were used to aspirate RBCs (200 Pa), imaged (Nikon TE300) with 40x objective, captured with Cascade CCD camera (Roper Scientific), and analyzed with ImageJ.

Time Lapse Microscopy. Phase-contrast imaging was performed in a humidified chamber at 37*C and 5% CO2 using an inverted microscope (Olympus IX-71) with a 40x objective (NA 0.6) and high-resolution CCD camera (CoolSNAP HQ; Photometrics). softWoRx [DeltaVision] was used for image-capture. DIC imaging was performed in a temperature-controlled chamber with THP-1 cultured in HEPES buffered RPMI, using an inverted microscope (Leica TCS SP5)

with a 63x water-immersion objective (NA 1.2). Time-lapse imaging was initiated when a RBC adhered to a macrophage. ImageJ was used to analyze dimensions of RBC during engulfment.

Confocal Microscopy. Macrophage and RBC were co-cultured in 4-cm2 Lab-Tek chambered coverglass (Nalge Nunc International) were imaged using an inverted microscope (Leica TCS SP5) with a 63x water-immersion objective (NA 1.2). Anti-Rabbit IgG conjugated to AlexaFluor647 was excited with a He Ne laser at 633 nm, and emission was collected in the range of 650-720. Phalloidin-AlexaFluor488 was excited with an argon laser at 488 nm, and emission was collected within 500-550 nm. DiIC18 was excited with DPSS laser at 561 nm, and emission was collected within 600-650 nm, and DAPI was excited with the multiphoton laser at 730 nm, and emission was collected between 400-460 nm. Bidirectional scanning with a correction factor of -27 was used with a line average and frame average of 3.

Western Blotting. THP-1 macrophages were plated at 2E5 cells per well of a 6 well plate (Corning), and fed RBC at a ratio of 1 macrophage to 20 RBC. RBC conditions were, native, native-CD47-block, GA-Discocyte, and GA-Discocyte with Blebbistatin (20 uM). Cells were lysed with ice-cold RIPA buffer supplemented with 1% protease inhibitor, 1% phosphatase inhibitor, and 1% Vanadate. For every 100 uL of lysate, 30 uL of LDS, and 5 uL of BME were added prior to heating on heating block for 10 min at 70*C in water. 1 x 6 well plate was lysed for each condition, and equal volume of lysate was loaded in each lane of 3-8% Tris Acetate gel. Proteins were transferred to PVDF membranes, and blocked with 5% milk in TBS (m/v). Membranes were blotted for pS1943 (rabbit, Cell Signaling) and Nonmuscle Myosin-IIA (rabbit pAb, Sigma), and probed with anti-rabbit-HRP secondary, followed by chromosensor detection.

Vesicle Preparation. Giant vesicles composed of 1-palmitoyl-2-oleoyl-Glycero-3 phosphocholine (POPC) (Avanti) with <1% DiIC18 were prepared by electroformation. 5 uL of POPC/DiIC18 stock (10 mg/mL) was transferred to cleaned ITO glass slides with a Hamiltonian syringe, spread over the glass with the syringe tip, dried in fume hood for 2h. ITO glass slides and spacer were assembled and fill with an osmotically adjusted sucrose solution (340 mOsm). The apparatus was then treated with a sinus wave with voltage of 1.4V (RMS) and frequency of 10 Hz for 1.5 hours. Vesicles were equilibrated to ambient conditions 1h before transferring to glass vial. For phagocytosis assays, GUVs were pre-incubated with 10 μl anti-RBC antiserum (30 min, RT).

Phagocytosis Assay (Microscopy). THP-1s were treated with 100 ng/mL phorbol-myristate-acetate (PMA), for 2 days. Blebbistatin pre-incubation used 20 μM Blebbistatin at 37*C for 1 hour prior to RBC addition. RBCs were fed to macrophage at a ratio of 20:1, then incubated for 45 min at 37*C. Then cells were rinsed with PBS and fixed with 4% Formaldehyde. Non-ingested RBCs were differentiated by bound anti-rabbit–AF488 antibody. The phagocytosis index was calculated by counting the number of phagocytosed RBCs ≥200 macrophages, and expressed as the number of engulfed RBC per macrophage. Results consistent were consistent across multiple donors (Fig. S4D).

Microscopy of Phagocytic Synapse. THP-1 Macrophage were cultured on Nunc LabTek chambers, co-incubated with opsonized RBCs as in *'Phagocytosis Assay (Microscopy)'*, washed and fixed with 4% Formaldehyde, treated with Phalloidin-TRITC, Hoechst, anti-Myosin IIA, and anti-rabbit-AF488. Images were acquired with an inverted microscope (IX71; Olympus) with a 60x (oil, 1.4 NA) objective using a cascade CCD camera (Photometrics). Image acquisition was performed with ImagePro (Media Cybernetics, Inc.). Intensity analysis of the phagocytic synapse was performed using imageJ with a 38 x 1 pixel box, where the synapse was aligned at the box center. Fluorescence intensity was normalized to the minimum signal, and averaged over ≥ 3 randomly selected synapses.

Competitive in vivo Phagocytosis Assay RBCs were rigidified and opsonized as in vitro phagocytosis assays above. CD47+ and CD47-blocked RBCs were pre-treated with distinct lipophilic-dyes (PKH27 or DiR), mixed 1:1, and 2x107 RBCs were injected via tail vein to NOD/SCID/Il2rg−/− mice (NSG), following a protocol approved by the IACUC at the University of Pennsylvania. 15 minutes post-injection spleens were isolated, washed, treated with RBC-Lysis-Bufer (Sigma 10min RT) and analyzed for IR intensity with a LI-COR Odysey (LI-COR). Flow cytometry differentiated splenic macrophage from splenocytes via Cd11b expression and each population was analyzed for RBC signal.

Statistical Analysis. All statistical analyses were performed using GraphPad Prism 4. Unless otherwise noted, all statistical comparisons were made by unpaired two-tailed Student t test and were considered significant if $P < 0.05$.

Supplemental Figure Legends

Table S1. **Rigidity and IgG Opsonization of Aged and Diseased RBC.** Increased rigidity, IgG opsonization, phagocytosis and in vivo symptoms are reported for senescence, blood bank storage, and a variety of RBC disease states.

Table S2. **Opsonization Conditions.** The various opsonization conditions used thoughout this work are quantitatively defined here. The concentration of the antiserum (Rockland 109-4139) is reported to be approximately 100 mg/mL. It has been reported that the mass fraction of gamma globulins (IgG) in antiserum is approximately 0.2[S59,S60] so that the IgG concentration in antiserum is approximately 20 mg/mL or ~100 μM.

Figure S1. **Glutaraldehyde and Malonyldialdehyde RBC bind SIRPA, anti-CD47, and anti-RBC similarly to Native RBC. (A)** Binding of saturating concentrations of soluble human-SIRPA-GST+ fluorescent anti-GST for detection, to human RBC treated with Glutaraldehyde (GA, 1 min at RT) shows no significant difference as compared to native RBC. Binding of saturating concentrations of high affinity mAb anti-CD47 (B6H12) also is independent of GA treatment. **(B)** Malonyldialdehyde (MDA) was synthesized as in studies by Jain and Hochstein[S61], the concentration was determined from known mass of reactants, and RBCs were treated with 0.3, 1.0, and 3.0 mM MDA for 1 hour at 37ºC as in studies by Hebbel & Miller[34], and binding of saturating concentrations of SIRPA-GST-Fluor was assessed by flow cytometry. Binding curves of the (**C**) SIRPA-GST + fluorescent anti-GST for detection, or (**D**) SIRPA-GST-Fluor that is directly labeled fusion protein, and (**E**) anti-CD47 for native and GA-Discs was quantified by flow cytometry. (**F**) Native RBC and GA-Discs were opsonized with antiserum, and bound IgG was quantified by flow cytometry. Note that compared to the physiologically relevant temperature and concentrations of MDA, GA was used for much shorter time at lower temperature but higher concentration, to give both a similar rigidification and a similar fold-increase in phagocytosis as the MDA treatment (**Fig. S2, Fig. S4D,E**). Crosslinking reactions that are run fast and cold will tend to crosslink existing complexes in place, thereby limiting diffusion-augmented assembly, and yield a more native but rigidified structure (analogous to quick-freeze solidification methods).

Figure S2. **Rigid Cells Show Reduced In Vivo Circulation, Reduced In Vitro Aspiration Speed, and enhanced Erythrophagocytosis. (A)** In studies by Jain *et al.*[33] rabbit RBC were treated with 0-80 μM Maldionylaldehyde (MDA) for 1 hour at 37ºC, and measurements of RBC deformability in bulk shear by ektacytometry demonstrated an exponential decay with MDA, Deformability Index (*DI)* = 100*exp(-[MDA]/17 μM), R^2=0.999. Inset: The in-vivo circulation half-life shows a power-law dependence on DI, fitting to $\tau_{half} = 5.2\ DI^2$. (**B**) GA treated RBCs were aspirated in micropipettes similar in size to phagocytic cups. Aspiration rate was quantified and normalized relative to the rate of native cell aspiration. The number of cells that were fully aspirated versus the number that became stuck at the pipette entrance was quantified (inset table).

Figure S3. **Quantitation of RBC and giant vesicle deformation, phagocytic force, and phagosome apposition during phagocytosis.** (**A**) During classical phagocytosis the hRBC is first pinched outside the macrophage, elongated by mid-engulfment, and finally spherical once engulfed (scalebar: 10 μm), and corresponding confocal images of RBC (anti-rabbit-AF647, red; Phalloidin-AF488, green) were quantified for length and length to width ratio. (**B**) (**i**) Time-lapse imaging of the contact point between macrophage and an opsonized Giant POPC-DiIC18 lipid vesicle shows that the vesicle membrane intensity increases in a manner that suggests macrophage pseudopods pinch the vesicle membrane (0 sec, left) causing vesicle rupture. (**ii**) In a second time-series, a vesicle is contacted by pseudopods of two macrophages, By 4 sec post-initial contact the macrophage has deformed the vesicle (**iii**, box-1, arrow) and by 24 sec post-initial contact the macrophage has gathered a portion of the ruptured vesicle (**iii**, box 2, arrow). (**iv**) The inset schematic depicts the observed vesicle deformation. The length and width of the vesicle as well as the corresponding change in mean intensity during the course of engulfment were quantified, where the decrease in vesicle area and increase in vesicle intensity (highlighted by pink box) highlight that the vesicle ruptures, followed by rapid aggregation of the lipid membrane in the surrounding medium (scalebars: 10 μm). (**C**) Green's strain Tensor (Eq.s 1 and 2) was used to relate deformations of Native RBCs to the force a macrophage exerts on a RBC during engulfment. The force imposed by macrophage was quantified throughout engulfment, and was found to have a maximum of ~50 pN. (**D**) Timelapse imaging allows for visualization of the spacious loosely apposed GA-Disc phagosome. The DIC intensity across the x and y axes (defined in the image at 95 sec) was quantified, and indicate the gap that is ≤3 μm. This spacious phagosome may act as a barrier to signaling via macrophage receptors that is dependent on binding to the target cell (scalebar: 5 μm).

Figure S4. **Interplay of Rigidity, Opsonization, and CD47-Inhibition in Macrophage Phagocytosis. (A)** Confocal imaging of Phalloidin stained F-actin fibers in macrophage that were fed CD47-blocked RBC (scale bar: 10 μm). (**B**) Imaging of actomyosin fibers in macrophage fed Native RBCs or GA-Discs with or without a Blebbistatin pretreatment (Myosin-II, green; F-actin, red, scalebar: 30 μm). (**C**) Immunoblots for nonmuscle myosin IIA heavy chain (upper two blots; also see Fig.3D-inset) and for pS1943-Myosin-IIA (lower two blots) using macrophage lysates after phagocytosis. Dephosphorylation of Myosin-IIA's S1943 is reported to correlate with the assembly of myosin-II fibers[S62], and so the blots were stripped of anti-myosin-IIA and reprobed with anti-pS1943. Quantitation of bands by densitometry shows that the intensity ratios of the ('assembled' 520 kDa band)/('monomeric' 230 kDa band) are always lower for pS1943 than for myosin-IIA. This supports the tentative conclusion that the high molecular weight band reflects more stable myosin assembly. (**D**) A flow cytometry based phagocytosis assay was performed on high antiserum opsonized GA-discs treated with 0-50 mM GA, and indicates that phagocytosis increases exponentially with glutaraldehyde concentration. (**E**) In studies by Hebbel and Miller[34], RBCs were treated with MDA at the indicated concentration for 2 hours at 37ºC, after which the percentage of RBC that were engulfed was quantified. (**F**) Ligation of CR1 has been reported to lead to an increase in RBC deformability[S63,S64], while aldehyde treatment increases RBC rigidity[S61]. CD47 inhibition of RBC phagocytosis by THP-1 macrophages was assessed for donors of diverse geographical origin that vary not only in malaria incidence (column 1[S65]) but also in frequency of a CR1 polymorphism caused by a single base change that correlates with reduced CR1 density (column 2[S66-S68]). Despite the strong potential for differences, no significant difference is found for the phagocytic ratio (CD47-blocked / CD47+ RBC) across donors for either native RBC (column 3) or GA-discocytes (column 4). For all donors CD47 blocking increased phagocytosis of native RBC but did not affect phagocytosis of GA-Discs. CR1 is also expressed on macrophages[S69], but microarray analysis of THP-1s suggests very low CR1 expression levels (data accessible at NCBI GEO database[70], accession GDS4256). 3D plots of phagocytosis assay results for (**G**) native RBC and (**H**) GA-Discs under a range of antiserum opsonization and anti-CD47 blocking treatments. (**I**) Highly opsonized and rigidified GA-discocytes (17 mM GA) were either CD47-blocked or not, stained with DiR, then injected via tail vein to NSG mice. Spleens were analyzed for IR intensity by LI-COR (excitation 800 nm). ~3 x 10^4 GA-Discs localized to each spleen independent of CD47-blocking, as determined by calibration with IR intensity analysis of a dilutions series of pre-injected blood.

Figure S5. **GA-Stomatocyte Phagocytosis. (A)** Phase contrast imaging of GA-Discocytes (left) and GA-Stomatocytes (right) show that GA-stomatocytes appear more rounded than GA-discocytes and have a smaller area of central pallor. (**B**) Binding of IgG to high antiserum opsonized native RBC and GA-stomatocytes is the same. (**C**) Similarly to Native RBC, and GA-Discocytes, GA-stomatocytes show binding of SIRPA-GST + fluorescent anti-GST for detection, is significantly higher than background, and is inhibited by pre-treatment with anti-CD47. (**D**) Anti-RBC IgG from purified anti-serum was used at same dilution as the high antiserum opsonization condition (Table S2). Inset: The amount of IgG bound to high antiserum and high IgG opsonized GA-discocytes, as quantified by flow cytometry, is the same. Uptake of pure IgG opsonized GA-Discocytes is low as compared to antiserum opsonized GA-discocytes (Fig 5A). CD47 blocking, led to significantly greater engulfment of the more rounded but rigid pure IgG opsonized GA-Stomatocytes, but had no effect on uptake of pure IgG opsonized GA-Discocytes. For all experiments (*$p < 0.05$; $n \geq 5000$ macrophage in duplicate, $\pm$ SD). (**E**) Time-lapse imaging of THP-1 phagocytosis of native RBC, GA-stomatocytes, and GA-discocytes was performed with and without CD47-blocking. Anti-CD47 blocking significantly decreases the time to complete phagocytosis of both GA-stomatocytes and native RBCs. In contrast, CD47 blocking increases the time to complete phagocytosis of GA-discocytes.

Supplementary References

1 Waugh RE, Narla M, Jackson CW, et al. Rheological Properties of Senescent Erythrocytes: Loss of Surface Area and Volume with Red Blood Cell Age. *Blood.* 1992;79(5):1351-1358.

2 Linderkamp O, Meiselman HJ. Geometric, Osmotic, and Membrane Mechanical Properties of Density-Separated Human Red Cells. *Blood.* 1992;59(6):1121-1127.

3 Snyder LM, Fortier NL, Trainor J, et al. Effect of Hydrogen Peroxide Exposure on Normal Human Erythrocyte Deformability, Morphology, Surface Characteristics, and Spectrin-Hemoglobin Cross-Linking. *J Clin Invest.* 1985;76(5):1971-1977.

4 Kameneva MV, Garrett KO, Watach MJ, et al. Red Blood cell aging and risk of cardiovascular diseases. *Clin Hemorheol and Microcirc.* 1998;18(1):67-64.

5 Bosch FH, Were JM, Schipper L, et al. Determinants of red blood cell deformability in relation to cell age. *Eur J Hematol.* 1994;52(1):35-41.

6 Kay MM. Isolation of the phagocytosis-inducing IgG-binding antigen on senescent somatic cells. *Nature*. 1981;289(5797):491-494.

7 Kay MM, Goodman SR, Sorensen K, et al. Senescent cell antigen is immunologically related to band 3. *Proc Natl Acad Sci U S A*. 1983;80(6):1631-1635.

8 Low PS , Waugh SM, Zinke K, et al. The role of hemoglobin denaturation and band 3 Clustering in Red Blood Cell aging. *Science.* 1985;227(4686):531-533.

9 Beppu M, Atsushi A, Nagoya M, et al. Binding of anti-band 3 autoantibody to oxidatively damaged erythrocytes. *J Biol Chem.* 1990;265(6):3226-3233.

10 Kannan R, Yuan J, Low PS. Isolation and partial characterization of antibody- and globin-enriched complexes from membranes of dense human erythrocytes. *Biochem J.* 1991;278:57-62.

11 Muller H, Lutz HU. Binding of autologous IgG to human red blood cells before and after ATP depletion. *Biochimica Biophys Acta.* 1983;729(2):249-257.

12 Wiener E, Hughes-Jones NC, Irish WT, et al. Elution of antispectrin antibodies from red cells in homozyogous beta-thalassaemia. *Clin Exp Immunol.* 1986;63(3):680-686.

13 Giuliani AL, Graldi G, Veronesi M, et al. Binding of anti-spectrin antibodies to red blood cells and vesiculation in various in vivo and in vitro ageing conditions in the rat. *Exper Gerontol.* 2000;35(8):1045-1059.

14 Hornig R, Lutz HU. Band 3 Protein clustering on human erythrocytes promotes binding of naturally occurring anti-band 3 and anti-spectrin antibodies. *Exp Gerontol.* 2000;35(8):1025-1044.

15 Selwyn JG. Heinz bodies in red cells after splenectomy and after phenacetin administration. *Br J Haematol*. 1955;1(2):173-183

16 Zheng Y, Chuen J, Cui T, et al. Characterization of red blood cell deformability change during blood storage. *Lab Chip.* 2014;14(3):577-583.

17 Frank SM, Abazyan B, Hogue CW, et al. Decreased erythrocyte deformability after transfusion and the effects of erythrocyte storage duration. *Anasthes and Analg.* 2013;116(5):975-81.

18 Luten M, Roerdinkholder-Stoelwinder B, Bost HJ, et al. Survival of the fittest?—survival of stored red blood cells after transfusion. *Cell Mol Biol.* 2004;50(2):197-203.

19 Dinkla S, Novotny VMJ, Joosten I, et al. Storage-induced chages in erythrocyte membrane proteins promote recognition by autoantibodies. *PLoS One.* 2012;7(8):1-9.

20 Luten M, Roerdinkholder-Stoelwinder B, Schaap NP, et al. Survival of red blood cells after transfusion: a comparison between red cells concentrates of different storage periods. *Transfusion.* 2008;48(7):1478-1485.

21 Beauge F, Stibler H, Borg S. Abnormal fluidity and surface carbohydrate content of the erythrocyte membrane in alcoholic patients. *Alcohol Clin Exp Res.* 1985;9(4):322-326.

22 Beauge F, Niel E, Hispard E, et al. Red blood cell deformability and alcohol dependence in humans. *Alcohol Alcohol.* 1994;29(1):59-63.

23 Stibler H, Beauge F, Leguicher A, et al. Biophysical and biochemical alterations in erythrocyte membranes from chronic alcoholics. *Scand J Clin Lab Invest.* 1991;51(4):309-319.

24 Sonmez M, Ince H, Yalcin O, et al. The effects of alcohol on red blood cell mechanical properties and membrane fluidity depends on their molecular size. *PLoS One.* 2013;8(9):e76579.

25 Setshedi M, Wands JR, Monte SM. Acetaldehyde adducts in alcoholic liver disease. *Oxid Med Cell Longev.* 2010;3(3):178-185.

26 Viitala K, Israel Y, Blake JE, et al. Serum IgA, IgG, and IgM Antibodies directed against Acetaldehyde-derived epitopes: relationship to liver disease severity and alcohol consumption. *Hepatology.* 1997;25(6):1418-1424.

27 Worrall S, de Jersey J, Wilce PA, et al. Relationship between alcohol intake and immunoglobulin A immunoreactivity with alcetaldehyde-modified bovine serum albumin. *Alcohol Clin Exp Res.* 1996;20(5):836-840.

28 Franklin Adkinson N, Busse WM, Bochner BS, et al. Middleton's Allergy: Principles and Practice. City: Mosby. 2008.

29 Guo R, Hu N, Machender R, et al. Facilitated ethanol metabolism promotes cardiomyocyte contractile dysfunction through autophagy in murine hearts. *Autophagy.* 2012;8(4):593-608.

30 Lewis G, Wise MP, Poynton, et al. A case of persistent anemia and alcohol abuse. *Nature Clin Practice*. 2007;4(9):521-526.

31 Ballard HS. The hematological complications of alcoholism. *Alcohol Health and Res World*. 1997;21(1):42-52.

32 Tsai M, Kita A, Leach J, et al. In vitro modeling of the microvascular occlusion and thrombosis that occur in hematologic diseases using microfluidic technology. *J Clin Invest*. 2012;122(1):408–418.

33 Tripette J, Loko G, Samb A, et al. Effects of hydration and dehydration on blood rheology in sickle cell trait carriers during exercise. *Am J Physiol Heart Circ Physiol.* 2010;299(3):H908-H914.

34 Fortier N, Snyder LM, Garver F, et al. The relationship between in vivo generated hemoglobin skeletal protein complex and increased red cell membrane rigidity. *Blood.* 1988;71(5):1427-1431.

35 Dong C, Chadwick RS, Schechter AN. Influence of sickle hemoglobin polymerization and membrane properties on deformability of sickle erythrocytes in the microcirculation. *Biophys J.* 1992;63(3):774-783.

36 Green MA, Noguchi CT, Keidan AJ, et al. Polymerization of sickle cell hemoglobin at arterial oxygen saturation impairs erythrocyte deformability. *J Clin Invest*. 1988;81(6):1669-1674.

37 Sorette MP, Lavenant MG, Clark MR. Ektacytometry measurement of sickle cell deformability as a continuous function of oxygen tension. *Blood.* 1987;69(1):316-323.

38 Nash GB, Johnson CS, Meiselman HJ. Mechanical properties of oxygenated red blood cells in sickle cell (HbSS) Disease. *Blood.* 1984;63(1):73-82..

39 Schluter K, Detley D. Co-clustering of denatured hemoglobin with band 3: Its role in binding of autoantibodies against band 3 to abnormal and aged erythrocytes. *Proc Natl Acad Sci U S A*. 1986;83(16):6137-6141.

40 Hebbel RP, Miller WJ. Phagocytosis of sickle erythrocytes: immunologic and oxidative determinants of hemolytic anemia. *Blood*. 1984;64(3):733-741.

41 Solanki DL. Erythrophagocytosis in vivo in sickle cell anemia. *Am J Hematol*. 1985;20(4):353-7.

42 Solanki DL, Kletter GG, Castro O. Acute splenic sequestration crises in adults with sickle cell disease. Am J Med. 1986;80(5):985-990.

43 Dondorp AM, Chotivanich KT, Fucharoen S, et al. Red cell deformability, splenic function, and anaemia in thalassaemia. *Br J Haematol*. 1999;105(2):505-508.

44 Ayi K, Turrini F, Piga A, et al. Enhanced phagocytosis of ring parasitized mutant erythrocytes: a common mechanism that may explain protection against falciparum malaria in sickle trait and beta-thalassemia trait. *Blood.* 2004;104(10):3364-3371.

45 Luzzi GA, Merry AH, Newbold CI, et al. Surface Antigen expression on plasmodium falciparum-infected erythrocytes is modified in alpha- and beta-thalassemia. *J Exp Med*.1991;173(4):785-791.

46 Mannu F, Arese P, Capellini MD, et al. Role of hemichrome binding to erythrocyte membrane in the generation of band 3 alterations in beta-thalassemia intermedia erythrocytes. *Blood*. 1995;86(5):2014-2020.

47 Aessopos A, Farmakis D, Tsironi M, et al. Hemodynamic assessment of splenomegaly in beta-thalassemia patients undergoing spenectomy. *Ann Hematol*. 2004;83(12):775-778.

48 Liu TZ, Lin TF, Hung IJ, et al. Enhanced susceptibility of erythrocytes deficient in G6PD to alloxin/glutathione-induced decrease in red cell deformability. *Life Sci*. 1994;55(3):PL55-60.

49 Cappadaro M, Giribaldi G, O'Brien E, et al. Early phagocytosis of glucose-6-phosphate dehydrogenase (G6PD)-deficient erythrocytes parasitized by plasmodium falciparum May explain malaria protection in G6PD Deficiency. *Blood*.1998;92(7):2527-2534.

50 Hamilton JW, Jones FG, McMullin MF. Glucose-6 phosphate dehydrogenase Guadalajara—a case of chronic non-spherocytic haemolytic anaemia responding to splenectomy and the role of splenectomy in this disorder. *Hematology*. 2004;9(4):307-309.

51 Rey J, Buffet PA, Ciceron L, et al. Reduced erythrocyte deformability associated with hypoargininemia during Plasmodium falciparum malaria. *Sci Rep*. 2014;4:3767.

52 Giribaldi G, Ulliers D, Mannu F, et al. Growth of Plasmodium Falciparum induces stage-dependent haemichrome formation, oxidative aggregation of band 3, membrane deposition of complement and antibodies, and phagocytosis of parasitized erythrocytes. *Br J Hematol*. 2001;113(2):492-499.

53 Buffet PA, Safeukui I, Deplaine G, et al. The pathogenesis of Plasmodium falciparum malaria in humans: insights from splenic physiology. *Blood*. 2011;117(2):381-392.

54 De Francheschi L, Sada S, Andreoli A, et al. Sickle cell disease and hyperreactive malarial splenomegaly (HMS) in young immigrants from Africa. *Blood*. 2005;106(13):4415-4417.

55 Norman FF, Rojas-Marcos J, Hermida-Donate JM, et al. Splenic infarction and malaria. *Trans R Soc Trop Med Hyg*. 2014;108(8):455-60.

56 Tano ZN, Filho CE, Bregano RM, et al. Hyperreactive malarous splenomegaly and aids: a case report. *Brazillian J Inf Dis* 2014;18(5):565-7.

57 Safeuki I, Bufet PA, Deplaine G, et al. Quantitative assessment of sensing and sequestration of spherocytic erythrocytes by the human spleen. *Blood*. 2012;120(2):424-430.

58 Masera G, Mieli G, Petrone M, et al. Transient aplastic crisis in hereditary spherocytosis. *Acta Hematol*. 2002; 63(1):28-31.

59 Turrini F, Mannu F, Arese P, Yuan J, Low PS, Cohen RM. Characterization of the Autologous Antibodies That Opsonize Erythrocytes With Clustered Integral Membrane Proteins. *Blood*. 1993;81(11):3146-3152.

60 Merrell K, Southwick K, Graves SW, et al. Analysis of Low-Molecular-Weight Serum Proteins Using Mass Spectrometry. *J Biomol Tech*. 2004;15(4):238-248.

61 Jain SK, Hochstein P. Polymerization of membrane components in aging red blood cells. *Biochem and Biophys Res. Commun*. 1980;92(1):247-254.

62 Alberts B, Johnson A, Lewis J, et al. Molecular Biology of the Cell. New York: Garland Science; 2007.

63 Glodek AM, Mirchev R, Golan DE, et al. Ligation of complement receptor 1 increases erythrocyte membrane deformability. *Blood*. 2010;116(26):6063-6071.

64 Manno S, Takakuwa Y, Nagao K, et al. Modulation of erythrocyte membrane mechanical function by beta-spectrin phosphorylation and dephosphorylation. *J Biol Chem*. 1995;270(10):5659-5665.

65 World Health Organization: World Malaria Report. 2013. Retrieved from http://kff.org/globaldata

66 Thomas BN, Donovito B, Cockburn I, *et al*. A complement receptor-1 polymorphism with high frequency in malaria endemic regions of Asia but not Africa. *Genes Immun*. 2005;6(1):31-36.

67 Katyal M, Sivasankar B, Ayub S, et al. Genetic and structural polymorphism of complement receptor 1 in normal Indian subjects. *Immunol Lett*. 2003;89(2-3):93-98.

68 Wilson JG, Murphy EE, Wong WW, et al. Identification of a restriction fragment length polymorphism by a CR1 cDNA that correlates with the number of CR1 on erythrocytes. *J Exp Med*. 1986;164(1):50-59.

69 Ghiran I, Barbashov SF, Klickstein LB, et al. Complement receptor 1/CD35 is a receptor for mannan-binding lectin. *J Exp Med*. 2000;192(12):1797-1808.

70 Kim MJ, Wainwright HC, Locketz M, et al. Caseation of human tuberculosis granulomas correlates with elevated host lipid metabolism. *EMBO Mol Med*. 2010;2(7):258-274.

Table S1. Rigidity and IgG Opsonization of Aged and Diseased RBC

RBC Condition	Likely Source of Damage	Increased Rigidity	Increased IgG Opsonization	Increased Phagocytosis	*in vivo* symptoms
Senescence	oxidation	S1-S5	18-19, 58, S6-S15	58, S7	58, S16
Storage	Additional Oxidation	S17-S18	S19-S20	74, 75	23, 45, S21
Alcohol Consumption	Acetaldehyde Production	S22-S25	S26-S29	S30	S31-S32
Sickle cell Disease	Increased Oxidation Sensitivity	S33-S39	S40-S41	S41	S42-S43
Beta Thalassemia		S35, S44	S45-S46	S45, S47	S44, S48
G6PD Deficiency		S49	S45, S50	545, S50	S51
Malaria	Infection	38, S52	S45, S53	S45, S53	S54-S57
Hereditary Spherocytosis	Loss of SA	25, S58	25	S59	25

Table S2. Opsonization Conditions

Opsonization Condition	Vendor, Cat No.	Dilution Factor
High Antiserum	**Rockland 109-4139 rabbit**	**1:10-1:30**
Intermediate Antiserum		**1:50**
Low Antiserum		**1:100**
Zero Antiserum		**na**
Purified Antiserum	**Rockland 209-4139 rabbit**	**1:10**

Conc. Antiserum (mg/mL)	Mass Fraction IgG	Conc. IgG (mg/mL)	Conc. IgG (μM)	Conc. IgG In High Antiserum (μM)
~100	0.2	~20	~100	~10

Figure S1 Glutaraldehyde and Malonyldialdehyde RBC Bind SIRPA, anti-CD47, and anti-RBC similarly to Native RBC

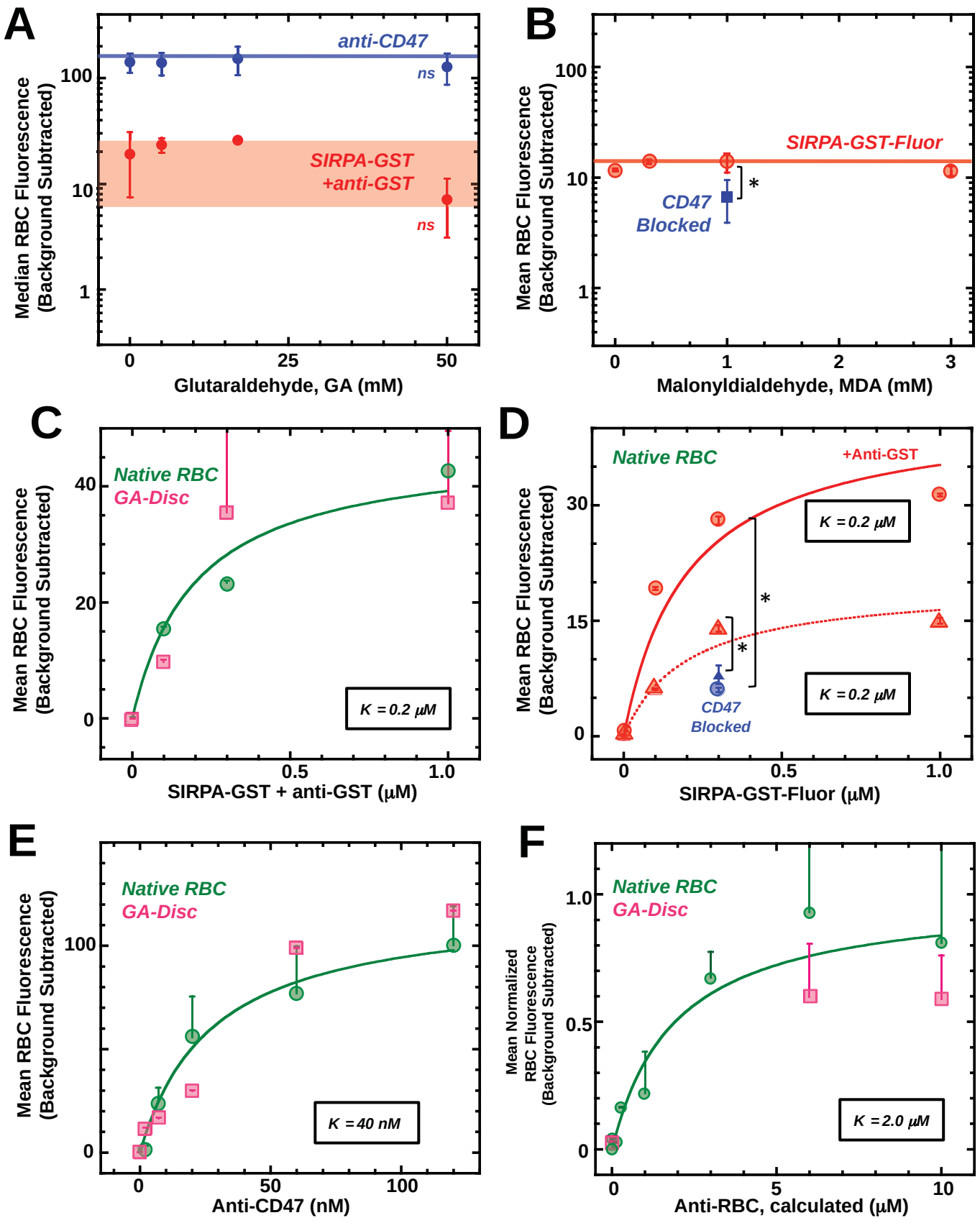

Figure S2. Rigid Cells Show Reduced In Vivo Circulation, and Reduced In Vitro Aspiration Speed

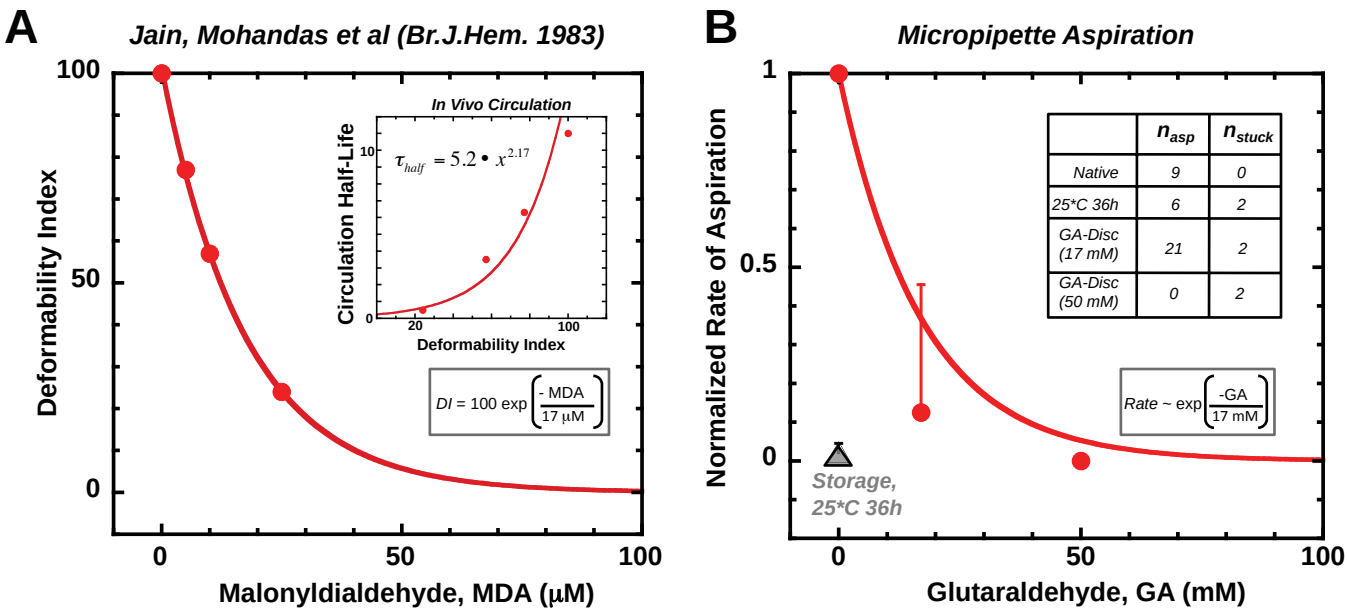

Figure S3 Quantitation of RBC and giant vesicle deformation, phagocytic force, and phagosome apposition during phagocytosis

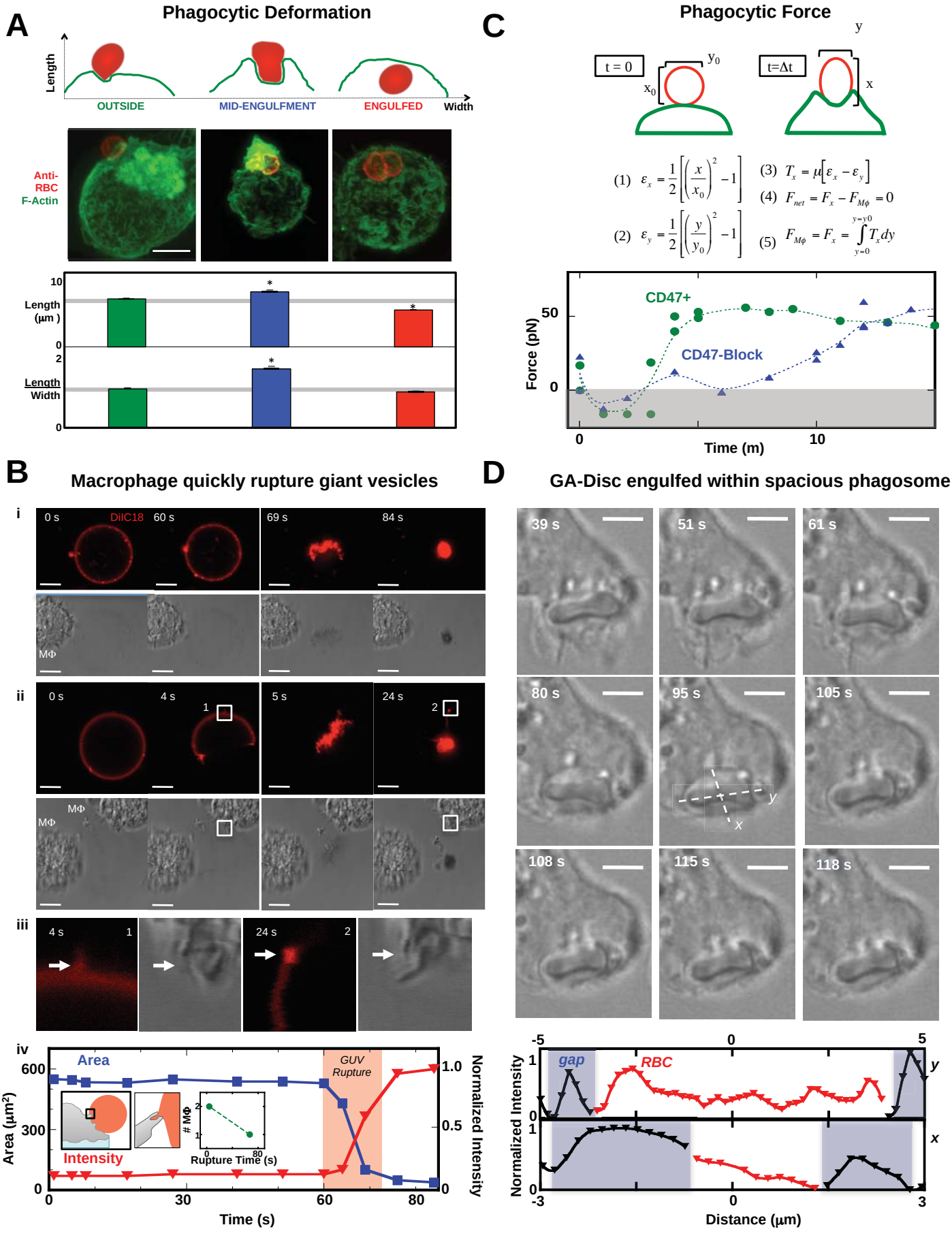

Figure S4 Interplay of Rigidity, Opsonization, and CD47-Inhibition in Macrophage Phagocytosis

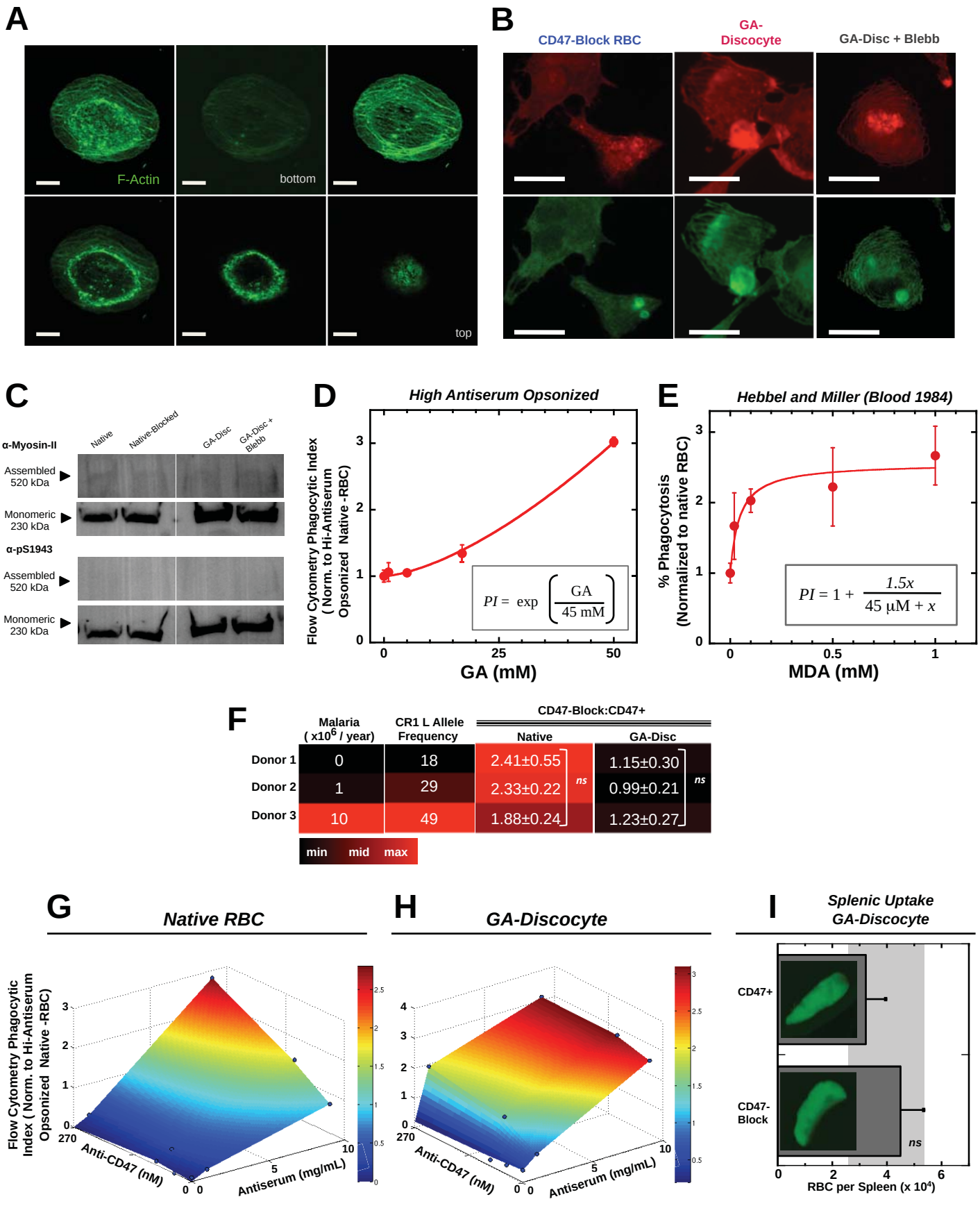

Figure S5. GA-Stomatocyte Characterization